Study on Heavy Metal Removal Performance of Different Ceramic Nano-Composite Tubular Membrane

The thesis submitted on partial fulfillment of the requirements of the degree of Master of Engineering in Chemical Engineering

Submitted by:

Umme Habiba

University Roll No: 002210302021

Exam Roll No: M4CHE24021

Reg. No. 163448 of (2022-23)

M.E in Chemical Engineering

Under the guidance of

DR. RANJANA DAS

Department of Chemical Engineering

In the partial fulfillment of the requirement for the degree of

MASTER OF CHEMICAL ENGINEERING

DEPARMENT OF CHEMICAL ENGINEERING

JADAVPUR UNIVERSITY

Jadavpur, Kolkata-700032

INDIA

July 2024

DECLARATION OF ORIGINALITY AND COMPLIANCE OF ACADEMIC ETHICS

I hereby declare that this thesis contains literature survey and original research work by the undersigned candidate, as part of his "**Master of Engineering in Chemical Engineering**" studies. All information in this document have been obtained and presented in accordance with academic rules and ethical conduct.

I also declare that, as required by these rules and conduct, I have fully cited and referenced all material and results that are not original to research work.

Name: **UMME HABIBA**

University Roll No: 002210302021

Exam roll no: M4CHE24021

Reg. No. 163448 of 2022-23

Thesis Title: **STUDY ON HEAVY METAL REMOVAL PERFORMANCE OF DIFFERENT CERAMIC NANO-COMPOSITE TUBULAR MEMBRANE**

Signature: Umme Habiba

Date: 28/08/24

CERTIFICATE

This is to certify that **UMME HABIBA**, final year student in Master of Chemical Engineering examination in the department of Chemical Engineering, Jadavpur University, bearing Registration No: 163448 of 2022-23 has successfully completed the thesis work entitled "**STUDY ON HEAVY METAL REMOVAL PERFORMANCE OF DIFFERENT CERAMIC NANO-COMPOSITE TUBULAR MEMBRANE**" under the guidance of **Dr. Ranjana Das** during her master degree curriculum. This work has not been reported earlier anywhere and can be approved for submission in partial fulfilment of the requirements for the Master of Engineering in Chemical Engineering.

Ranjana Das 28/08/2024

Dr. Ranjana Das

Thesis Supervisor

Chemical Engineering Department

Jadavpur University

Kolkata – 700032

Dr. Ranjana Das for
Associate Professor
Chemical Engineering Department
Jadavpur University
Kolkata - 700032

Ratna Dutta 29/08/24

Prof. (Dr.) Papita Das (H.O.D)

Chemical Engineering Department

Jadavpur University

Kolkata – 700032

HEAD (Officiating)
CHEMICAL ENGINEERING DEPARTMENT
JADAVPUR UNIVERSITY
Kolkata-700 032

Dipak Laha 29.8.24

Dean (FET)

Jadavpur University

Kolkata – 700032

DEAN
Faculty of Engineering & Technology
JADAVPUR UNIVERSITY
KOLKATA-700 032

CERTIFICATE OF APPROVAL

This thesis is hereby approved as the creditable study of an engineering subject carried out and presented in a manner satisfactory to warrant its acceptance as prerequisite to the degree for which it has been submitted. It is understood by this approval that the undersigned don't endorse or approve any statement made, opinion expressed or conclusion drawn therein but approve the thesis only for purpose of which it is submitted.

Umme Habiba

Umme Habiba

Department of Chemical Engineering

Jadavpur University

Acknowledgement

With immense please, I, Umme Habiba presenting “study on heavy metal removal performance of different ceramic nano-composite tubular membrane” thesis as a part of curriculum of M.E chemical engineering. I would like to express my special thanks of gratitude to our HOD Dr. Papita Das for giving me the opportunity to do this project and for his valuable suggestion and direction to accomplish the study.

I am greatly indebted to my thesis supervisor Dr. Ranjana Das for providing me with definite direction, professional guidance, and constant encouragement from the beginning of the work and moral support in many ways during study period.

I acknowledge the help, advice and guidance rendered by Research Scholar of Membrane Separation Lab Mr. Somakraj Banerjee and Aishwarya Das.

I am also thankful to the senior researchers and the other lab mates of the Membrane Research Laboratory who not only made the lab feel like home, but also helped me with minute details and suggestions which helped me carry out the project smoothly and understand my shortfalls too.

I am also grateful to all the colleagues of the Master of Engineering in Chemical Engineering 2024 batch. I am also very thankful towards my parents and my husband for their consistent support in every possible way.

ABSTRACT

The experimental investigation was carried out to study the removal of heavy metal contaminations from drinking water by synthesizing the mesoporous Mg–Al–Ti composite oxide nanoparticles and incorporating them into three different MMM layers on ceramic membranes. There are many heavy metals present in drinking water but we focused on arsenic, chromium, cadmium, and lead removal. Heavy metals have many adverse effects on the human body when consumed. There are many water purification techniques available such as Reverse Osmosis, Ultra-filtration, Microfiltration, and Nano-filtration for removing heavy metal contaminants from drinking water still none can remove arsenic efficiently from drinking water. The permissible limit of arsenic in drinking water is 10 ppb. Yet, a single process has not been developed that can bring arsenic-contaminated drinking water into the permissible limit suggested by the World Health Organization (WHO). Unlike other heavy metal removal methods, adsorption removes 95 % of arsenic from drinking water which is the highest removal rate in all available water purification techniques. Hence, we have chosen the adsorption process in the arsenic removal study. The planned methods are the synthesis of the PSF blend membrane, the In-situ formed membranes, and the PVA membrane by sol-gel method. The arsenic removal performances can be determined by characterization of all three mixed matrix membranes. After doing several tests like heavy metal ions competition, FESEM analysis, XRD analysis, contact angle, pure water flux, pH testing, anti-fouling test, long-term filtration, regeneration, and anti-bacterial property test. We concluded that NPs adsorption capacity for multi-metal (As, Pb, Cr, Cd) ions in binary, ternary, and total heavy metal batch setup shows excellent removal % (> 80 to 90 %) in all concentrations. The Arsenic adsorption properties of NPs incorporated MMMs in the effect of pH showed a 99 % removal percentage in all ranges of pHs. Membrane contact angles 25.06º (In-situ), 69.83º (PSF), and 35.58º (PVA) state the hydrophilic properties of the membranes. FRR 79 % of PSF, 87 % for In-situ, and 89.87 % for PVA membrane shows good anti-fouling properties of all MMMs. Long-term filtration shows a breakthrough volume of 4.5 L while filtering 100 ppb As a solution and the flux is declining with the addition of several filtration cycles. However after regeneration of the spent membrane, long-term filtration showed breakthrough volume of 2.5 L. The regeneration was confirmed with the increase in flux of the

spent membrane. In the anti-bacterial property test in-situ membrane showed better results than the other two membranes, altogether all three MMMs showed good anti-bacterial properties. Successful positive inhibitory zone, > 99 % E.coli removal percentage, and > 99.99 % removal of colony forming units (CFU/ml) in the filtration process confirmed the anti-microbial resistance. With its multi-functionality, these membranes hold great potential for practical water treatment applications.

Content Pages

Chapter 1

Introduction

1.1 General discussion.
1.2 Heavy metals.
1.3 Sources of heavy metal
1.3.1 Natural sources
1.3.2 Antropogenic sources
1.4 Sources of some typical heavy metals in water
1.5 Arsenic contamination in West Bengal ground water.
1.6 Arsenic removal methods
1.7 Mixed Matrix Membrane.
1.8 Sol-gel method.

6 to 18

Chapter 2

Aims and objectives

2.1 Objectives
2.2 Planes of work
2.3 Process Flow
2.4 Working principle of the unit.

19 to 23

Chapter 3

Literature review

3.1 Heavy metal ions competition
3.2 Pure water flux

24 to 33

3.3 pH testing
3.4 Anti-fouling
3.5 Long-term filtration
3.6 Regeneration
3.7 Anti-fouling

Chapter 4
Material & Methods

4.1 Materials
4.2 Methods
4.2.1 Synthesis of mesoporous Mg-Al-Ti composite oxide nanoparticles
4.2.2 Synthesis of MMMs

4.2.2.1 Preparation of polysulfone blend ceramic membrane
4.2..2 Preparation of In situ formed membrane
4.2.2.3 Preparation of PVA membrane
4.3 Characterization
4.3.1 TEM Analysis
4.3.2 XPS Analysis
4.3.3 BET Analysis
4.3.4 FESEM Analysis **34 to 55**
4.3.5 XRD Analysis
4.3.6 Contact Angle
4.3.7 ICP-OES
4.3.8 UV Visible Spectroscopy
4.3.9 Heavy metal ions competition
4.3.10 Pure water flux
4.3.11 pH Testing
4.3.12 Anti-fouling
4.3.13 Long Term Filtration

4.3.14 Regeneration,

4.3.15 Anti-Bacterial,

4.3.15.1 Disk diffusion assay

4.3.15.2 Biofilm Inhibition assay

4.3.15.2a Qualitative examination

4.3.15.2b Qualitative examination

4.3.15.3 E.coli filtration experiment

4.3.15.4 Solid surface antimicrobial activity

.

Chapter 5

Results and discussion

5.1 Characterization of nanoparticles

5.1.1 Adsorption isotherm

5.1.2 BET Analysis

5.1.3 XPS Analysis

5.1.4 XRD Analysis

5.1.5 TEM Analysis

5.1.6 Heavy metal ions competition, **56 to 78**

5.2 Characterization of MMMs

5.2.1 FESEM Analysis

5.2.2 XRD Analysis

5.2.3 Contact Angle

5.2.4 Pure water flux

5.2.5 pH Testing,

5.2.6 Anti-fouling

5.2.7 Long Term Filtration

5.2.8 Regeneration

5.2.9 Anti-Bacterial

5.2.9.1 Disk diffusion assay

5.2.9.2 Biofilm Inhibition assay

5.2.9.3 E.coli filtration experiment

5.2.9.4 Solid surface antimicrobial activity

Chapter 6

Conclusion **79**

Chapter 7

References **80 to 86**

LIST OF FIGURES

Figure No.	Caption
01	The geomorphic map of the Bengal besin and surrounding.
02	Mixed matrix Membrane.
03	Overview of sol-gel method process and products.
04	Flow chart of plan of work.
05	Ultra filtration unit.
06	Process flow of filtration unit.
07	Image of prepared MMMs.
08	Schematic diagram of a modern Tem.
09	Schematic diagram of XPS.
10	Schematic diagram of FESEM.
11	Schematic diagram of XRD.
12	Diagram of ICP-OES.
13	Schematic diagram of UV-Visible Spectroscopy.
14	Multi metal adsorption.
15	Disk diffusion assay.
16	a)Adsorption Isotherm of NPs, b) BET Analysis of NPs, c) XPS Analysis of NPs, d) XRD Analysis of NPs.
17	Images of TEM and EDX spectrum of NPs.
18	Removal percentage of binary multi metal competition.
19	Removal percentage of ternary multi metal competition.
20	Removal percentage of Total heavy metal

	competition.
21	Surface and cross-sectional FESEM images of all three MMMs.
22	FESEM & EDX mapping images of all three MMMs surface.
23	FESEM & EDX mapping after As adsorption.
24	XRD images of MMMs.
25	Contact angle of unmodified and all three MMMs.
26	Flux Recovery of all three MMMs at different pressure.
27	As concentration in pH (left), As removal percentage in different pH (right).
28	a)Water flux recovery of the MMMs before and after BSA permeation(left), b)fouling resistance ratios of the MMMs.
29	Long-term filtration of in-situ membrane.
30	Regeneration of in-situ membrane in NaOH solution.
31	Disk diffusion asaay.
32	Qualitative Examination
33	Quantitative Examination.
34	CFU count of MMMs after filtration (left), bacterial removal percentage of MMMs (right).
35	Microbial cell viability inhibition in time variant of all three MMMs.
36	Antimicrobial activity of all membrane's surface.

LIST OF TABLES

Table No.	Caption
01	Effects of heavy metals on human body and their permissible limit by WHO.
02	Method used for arsenic removal.
03	Fouling resistance ratios of MMMs.
04	CFU Count of MMMs after filtration.
05	Bacterial removal percentage of MMMs.
06	CFU count of membranes in 10&100 times dilutions.

NOMENCLATURE

nλ	Bragg's Law
J_w	Water Flux
FRR (%)	Flux Recovery Ratio Percentage
R_t(%)	Total Removal Percentage
R_r(%)	Reversible Fouling Percentage
R_{ir}(%)	Irreversible Fouling Percentage
Q_e	Adsorption Capacity

INSTRUMENT CREDENTIALS

Name of Equipment	Manufacturer
Weight balance	Sartorius
D.I water system	Sartorius & Milipore System
Magnetic Stirrer	Tarson
Ultrasonicator	Sartorius
Ph Meter	Sartorius, Lab Man & Hanna.
FESEM	ZEISS, Italy
Vortex	REMI
XRD	Malvern Panalytical
ICP-OES	PerkinElmer
Ultra filtration unit	Need Innovation
Temperature Controller	G.B Enterprise
Muffle Furnace	Concept International
Hot Air Oven	G.B Enterprise & Other Local made.
Laminar Flow	Filtech (India)
Auto clave	Esteem Autoclaves
TEM	Jeol India Pvt.Ltd.
B.O.D Incubator	Meditech Technologies India Pvt.Ltd.
UV-Vis	Yatherm Scientific
Centrifuge	SKYlab
BET	HORIBA

ABBREVIATION

WHO	World Health Organization
OES-ICP	Inductively Coupled Plasma – Optical Emission Spectrometry
FESEM	Field Emission Scanning Electron Microscope
XRD	X-Ray Diffraction
TEM	Transmission Electron Microscope
IOCS	Iron Oxide Covered Sand
NP	NanoPyto remediation
RO	Reverse Osmosis
PG	Pressure Gauge
TG	Temperature Gauge
UF	Ultra Filtration
PVA	Poly Vinyl Alcohol
BSA	Bovine Serum Albumin
MMM	Mixed Matrix Membrane
HNT	Halloysite Nano Tubes
MWCO	Molecular Weight Cut Off
CA	Contact Angle
PBS	Phosphate Buffer Solution
CV	Crystal Violet
NB	Nutrient Broth
CFU	Colony Forming Unit

CHAPTER 1

1.0 INTRODUCTION

In this part we will be discussing about

- Heavy metal pollution in drinking water.
- Heavy metal and its characteristic features
- Various sources of heavy metal
- Sources of some typical heavy metals
- Effects of heavy metals on human body
- Arsenic contaminations in west Bengal.
- Outline of arsenic removal methods
- Basis of selection of efficient removal process
- Review on MMM
- Brief outline of Sol gel method

1.1 General Discussion

Water is one of the primary sources of human survival. According to the rule of three, a person can't survive three minutes without air, three days without water, and three weeks without food. This proves the importance of water for human survival. It is a known fact that the earth's surface is covered with 71 % of water which includes all water bodies such as oceans, lakes, and rivers, etc and the oceans alone hold 96.5 % of the total water on Earth. It is also worth mentioning that 3 % is fresh water and only about 1.2 % is drinkable. However, the same water that gives life to humans may also kill them, and this is mostly due to human intervention. As the rate of global population growth, scientific advancements, and subsequent growth in industrial and agricultural activities increases, water pollution has become one of the most significant worldwide concerns. More than 150 million people worldwide are at risk due to drinking water contamination, which also claims the lives of more than 20 million people each year [1, 2]. Potentially the most dangerous water contaminants are the toxic ones, and their environmental pollution has become a global issue. Since their entry into the biological cycle causes fundamental changes in natural and human ecosystems. Heavy metals have atomic numbers greater than 20 and densities greater than 5 g/cm^3 [1]. Some of these metals are necessary for the body to operate normally, when they enter the body in excessive amounts, both directly and indirectly through the soil, water, and air, they have negative health impacts because of their cumulative nature. So, it's very crucial to keep their quantity under control. It is a shame that despite living in a world of growing technologies one of the basic needs of human survival 'drinking water' is still not under the permissible limit suggested by the World Health Organization (WHO) which is 10 ppb. Predominantly, there are 4 types of contaminations in water which are physical, chemical, biological, and radiological [3]. Physical contaminations include suspended materials present in lakes, rivers, and streams from soil erosion. Chemical contaminations include salts, pesticides, nitrogen, metals, etc. Biological contaminations include bacteria, viruses, parasites, etc. Radiological contaminations include uranium, plutonium, and cesium. Some of the contaminations are natural and some are manmade caused by wastes from sewage, agricultural chemicals, and industries. Here in this study, our investigation is centered on chemical contaminations in water, particularly heavy metals.

1.2 Heavy metals

One of the necessities 'drinking water' is among the most polluted things on Earth these days. With the increasing population human needs are also increasing and to meet the needs the supply has to be increased which is causing more industrial development and eventually the pollution is increasing. One of the major pollutants from industrial wastes is the release of heavy metals and metalloid contaminants in water bodies. Heavy metals have a higher density than water, are toxic, and are nonbiodegradable. Even mild exposure to heavy metals is hazardous to human health. There are many different types of heavy metal oxides and ions present in water. The popular heavy metals ions are arsenic (As), cadmium (Cd), chromium (Cr), lead (Pb), zinc (Zn), copper (Cu), nickel (Ni), mercury (Hg), etc and the common heavy metals are silver (Ag), iron(Fe), manganese (Mn), molybdenum (Mo), boron (B), calcium (Ca), antimony (Sb), cobalt (Co), etc. Some of these can be removed easily and some are difficult to remove from water. The removal process for the majorites of these heavy metals has already been developed excluding 'Arsenic'. There is still not a single water treatment process available that can be claimed to remove arsenic efficiently from water. Arsenic is carcinogenic and it has many other health effects once entered the human body. It is not only dangerous for humans but also for marine life and plants. One of the major sources of arsenic entering the human body is the consumption of contaminated drinking water but that is not the only source. Arsenic can also enter humans by consuming fish exposed to arsenic in water.

1.3 Sources of heavy metals

We believe that the heavy metals are only artificial which is not true. Actually some heavy metals are naturally present in earth's crust and some are artificial. There are two main sources by which the heavy metal contamination happens one is Natural sources and the other is anthropogenic sources [4, 5]. Explained below in details

1.3.1 Natural Sources:

There are many physical conditions in the nature by which directly or indirectly the heavy metals are contaminating the ground water and drinking water. Geological formations of Sedimentary

and volcanic rocks are one the major natural sources. Due to the strokes of river and ground water on the geological formations the heavy metals leaches out in the water and gets contaminated.

1.3.2 Anthropogenic Sources:

With rise in the industrialization, the demand of metal extraction and use of heavy metals in the industries has also increases. Due to human activities like smelting or treating of the ores of metals, mining, discharging industrial and domestics wastes, use of pesticides in agriculture the ground water and drinking water gets contaminated by heavy metals

1.4 Sources of some typical heavy metals in water [2]

Sources of lead (Pb) in ground water are lead-based batteries, solder, alloys, cable sheathing pigments, rust inhibitors, ammunition, glazes, and plastic stabilizers. Sources of arsenic in ground water are electronics and glass production. Sources of chromium (Cr) are steel and pulp mills and tanneries. Sources of cadmium (Cd) are batteries, paints, steel industry, plastic industries, metal refineries, and corroded galvanized pipes. Sources of zinc (Zn) are brass coating, rubber products, some cosmetics, and aerosol deodorants. Sources of copper (Cu) are corroded plumbing systems, electronic and cables industry. Sources of mercury (Hg) are electrolytic production of chlorine and caustic soda, runoff from landfills and agriculture, electrical appliances, Industrial and control instruments, laboratory apparatus, and refineries. Sources of nickel (Ni) are stainless steel and nickel alloy production. And when these harmful heavy metal gets in contact with human body, the toxicity of these heavy metals have adverse effects on human health. Some of the health effects of heavy metals on human body is mention briefly below in (**Table 1**)

Table No 1: Effects of heavy metals on human body and their permissible limit by WHO [2]

HEAVY METAL	EFFECTS ON HUMAN BODY	PERMITTED AMOUNT(µg)
Lead (pb)	Bones, liver, kidneys, brain, lungs, spleen, immunological system, hematological system, cardiovascular system, and reproductive system.	10
Arsenic (As)	Skin, lungs, brain, kidneys, metabolic system, cardiovascular system, immunological system, and endocrine.	10
Copper(Cu)	Liver, brain, kidneys, cornea, gastrointestinal system, lungs, immunological system, and hematological system.	2000
Zinc (Zn)	Stomach cramps, skin irritations, vomiting, nausea, and anemia, and convulsions	3000
Chromium (Cr)	Skin, lungs, kidneys, liver, brain, pancreas, tastes, gastrointestinal system, and reproductive system.	50
Cadmium (Cd)	Bones, liver, kidneys, lungs, testes, brain, immunological system, and cardiovascular system.	3
Mercury (Hg)	Brain, lungs, kidneys, liver, immunological system, cardiovascular system, endocrine, and reproductive system.	6
Nickel (Ni)	Lung, kidney, gastrointestinal distress, pulmonary fibrosis, and skin.	70

1.5 Arsenic contamination in West Bengal ground water:

Arsenic occurs naturally in the oxidation state of arsenate, arsenite, elemental arsenic, and arsine. Among all arsenite and arsenate are dominantly present in ground water. In India arsenic

contamination in groundwater in West Bengal was first detected in 1978, and around 16.66 million people (according to the 2001 census) in 8 districts in West Bengal are at risk [6,7]. High-level arsenic was detected in the shallow aquifer-tube wells of the basin in the late 20th century [6]. The source of the arsenic is geological. Bore-hole sample analyses show high arsenic concentrations only in soil layers rich in iron pyrites [7]. It has been reported that more than 50 million people living along the Ganga–Brahmaputra basins are affected by the high levels of arsenic in drinking water. High arsenic groundwater has been observed mainly in these districts of North 24 Parganas, Burdwan, Howrah, Hooghly, Kolkata, and Nadia [8]. The highest concentration of arsenic in groundwater was reported from Burdwan region followed by Kolkata [9]. This proves that most arsenic contamination is in areas surrounding the Bengal basin. In **(Fig.1)** map of the Bengal basin, we can see the surrounding areas. The white line encircles the regions with high-As groundwater in the shallow aquifers.

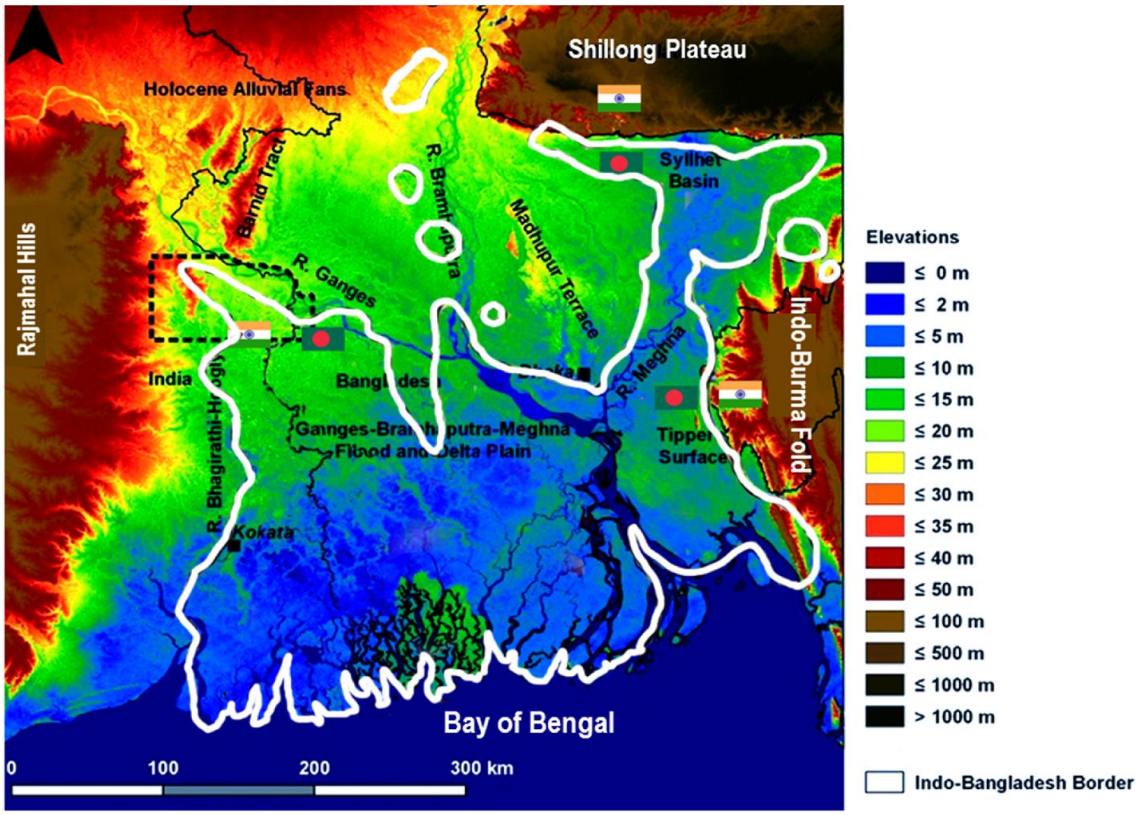


Figure 1. The geomorphic map of the Bengal basin and surroundings [10]

1.6 Arsenic removal methods:

Over the years, the need for arsenic and other heavy metal removal has led to the development of membranes with advanced technologies. After extensive studies and research in laboratories, the researchers have found different methods for removing arsenic from drinking water. Some of the arsenic removal methods currently in use are ion exchange, phytoremediation, adsorption, phytobial remediation, chemical precipitation, electrokinetic method, and electrocoagulation [1]. Even though all the methods can remove arsenic they have some drawbacks which are mentioned in (**Table 2**) the percentage of arsenic removal in each method has also been mentioned in the table. With the information and data provided in **Table No. 2**, we can conclude that adsorption is the most effective method that can remove arsenic from drinking water. Hence, the adsorption process was selected to remove arsenic contaminants from the drinking water.

Table No.2: Methods used for arsenic removal [1]

Methods	**Mechanism**	**Advantages**	**Disadvantages**	**Removal efficiency**
Adsorption	Use of solid to eliminate substances from a gaseous or liquid solutions	Secure operation handling; flexibility; low cost; sludge-free; high removal efficiency	Sorbents need replacement after adsorption bed gets too saturated and exhausted; eventually wholly loses the capacity for separation; not self-monitoring; sorbents have a	95%; The adsorption capacity of 136 mg/g and 189 mg/g was recorded with iron oxide covered sand (IOCS) and magnetic nano particles from tea waste used as an adsorbent.

			low specific surface area when using metal oxides; suitable for wastewater only with low arsenic concentrations	
Ion Exchange	Solid phase ions shared with equal ion numbers from contaminated water	Total removal and recuperation of metal subjects; limited toxic sludge production	Must be rejuvenated regularly to ensure complete removal; costly; each exchanger is specific for an arsenic species; Unfavourable order of selectivity; the resin is more responsive for natural anions	97.9% in the pH range from 3.5 to 7
Pyto- remediation	Utilises plants to address soil contamination	Eco-friendly and have high economic value; occurs naturally by using plants to assimilate	Time-consuming process; climate and tropical zone affect most of the hyper	99.9%

		arsenic from soil; prevents contaminant spreading; land restoration	accumulating plants; microbes produce additional toxic materials; lacks extensive applications; Hazardous pollutants interact with metabolic processes of plants and thereby hinder their growth and development	
Nanopytoremediation (NP)	The use of nanoparticles produced to reduced heavy metals or involving higher plants The activity of microbes and plants together is enhanced with nanoencapsulated enzymes	Improve phytoremediation efficiency; promoting in-situ remediation; increase in the degradation of pollutants into less toxic forms; cost effectiveness		99.9%
Pytobial Remediation	Uses interactions between plants	Eco-friendly; inexpensive;		99.9%

	and microorganisms, which can improve plant sequestration properties by enhancing rhizospheric metal absorption	enhances phytoremediation speed; modulates plant defence responses to stress factors, improves soil structure;assists in biological control of phytopathogens and plant growth; Is important in nutrient cycling;		
Chemical precipitation	Forms a separable solid substance from a solution;removes dissolved (ionic) metalsfrom solutions, such as processed wastewaters that contain toxic metals.	Simple and effective; specific components removed	Invariably forms silt; high processing costs	95%
Electro kinetic process	Works on fine-grained contaminated soils	Cost-effective in removal of a wide array of heavy metals.	Only works on a small portion of the soil at one time	90%
Electro-Coagulation	An alternative	A novel and	Not suitable and	99.9%

	solution to chemical precipitation; metallic cations directly produced by application of a current amid iron electrodes to liquefy soluble anodes in the waste treated	promising drinking-water arsenic removal strategy;efficient; relatively less cost;easy maintenance; operates with locally available materials	effective for extracting trivalent arsenic; producing contained sludge with high energy consumption; vastly affected by coagulant form and dose, solution pH and other competing anion availability	
Membrane technology	The membrane structure act as a selective barrier, that allows molecules to pass through with the help of a driving force produces large residual volumes.	High efficiency; low energy consumption; high filtration performance; used for various separation techniques	High costs high rejection of water	96%

1.7 Mixed matrix membrane:

To overcome a particular membrane's challenges such as to improve flux, rejection, selectivity, anti-fouling, and anti-bacterial properties the mixed matrix membrane method is used. As shown in **Figure (2)** MMMs are composite membranes made by combining an inorganic or inorganic-organic hybrid material in the form of micro or nanoparticles (the discrete or dispersed phase; additive or filler) and a polymer matrix (the continuous phase).

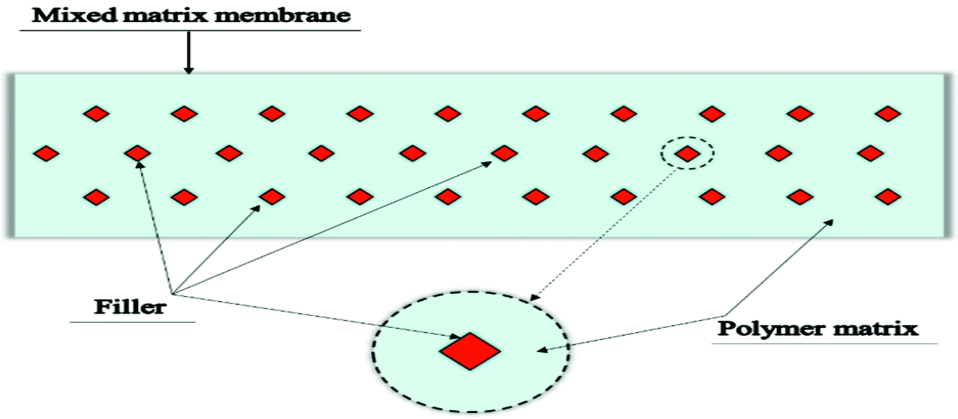


Figure 2. Mixed Matrix Membrane [11]

By using two materials with different transport properties, such membranes have the potential to combine synergistically the easy processability of polymers and the superior gas-separation performance of porous filler materials. MMMs may provide separation properties which can be above the Robeson upper bound by overcoming the trade-off between the selectivity and permeability that is typical for pure polymer membranes. Since a MMM is the dispersion of filler particles in a polymeric matrix, the properties of both the polymer and filler affect the separation performance. The chemical structure, surface chemistry, particle size distribution, and aspect ratio are other important factors of a filler material [12].

1.8 Sol-gel method:

The sol-gel process is a more wet chemical method for the synthesis of various nanostructures, especially metal oxide nanoparticles. In this method, the molecular precursor are usually metal alkoxide which is dissolved in water or alcohol and converted to gel by heating and stirring by

hydrolysis/alcoholysis. Since the gel obtained from the hydrolysis/alcoholysis process is wet or damp, it should be dried using appropriate methods depending on the desired properties and application of the gel. For example, if it is an alcoholic solution, the drying process is done by burning alcohol. After the drying stage, the produced gels are powdered and then calcined. The sol-gel method is a cost-effective method and due to the low reaction temperature there is good control over the chemical composition of the products. The sol-gel method can be used in the process of making ceramics as a molding material and can be used as an intermediate between thin films of metal oxides in various applications. The basis of the sol-gel method is the production of a homogeneous sol from the precursors and its conversion into a gel. The solvent in the gel is then removed from the gel structure and the remaining gel is dried. The properties of the dried gel depend significantly on the drying method. In other words, the "removing solvent method" is selected according to the application in which the gel will be used. Dried gels in various ways are used in industries such as surface coating, building insulation, and the production of special clothing. It is worth mentioning that, by grinding the gel by special mills, it is possible to achieve nanoparticles [13]. **Figure (3)** shows an overview of the types of processes that can be performed by the sol-gel method and the products derived from them.

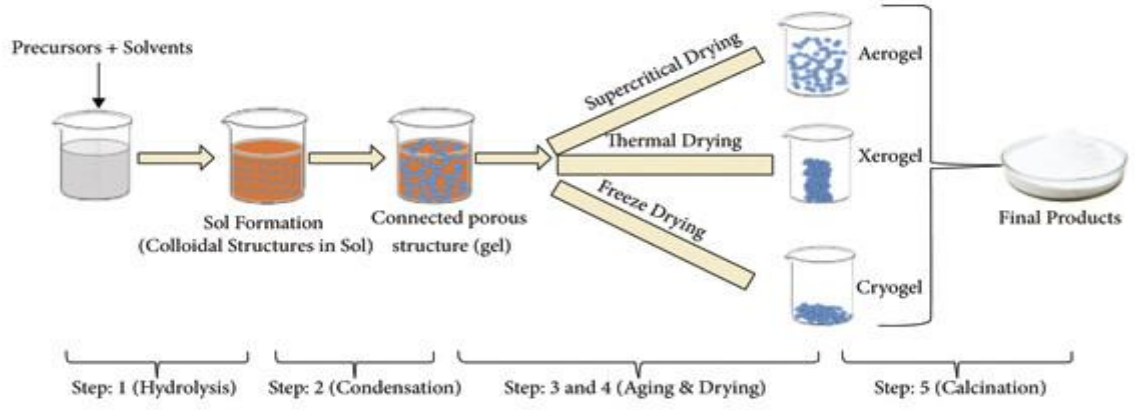


Figure 3. Overview of sol-gel method processes and products. [13]

Chapter 2

2. AIMS AND OBJECTIVES

In this chapter, we will be discussing the overall direction of the research work and the specific targets that are to be achieved at the end of the research work. For that, we have mentioned our plan of work in this chapter and discussed it in detail. We have also discussed the process flow and working principle of the ultra-filtration unit.

2.1 Objectives:

- Synthesis of mesoporous Mg-Al-Ti composite oxide nanoparticles for the removal of heavy metal contamination from drinking water.
- Synthesis of Mg-Al-Ti oxide incorporated MMM to increase the adsorption capacity of the membrane.
- To develop a membrane that can be used in households for heavy metal removal.
- To develop a technology that is both economically feasible and environment-friendly feasible.
- To investigate the different heavy metals removal performance in different coatings of ceramic membranes.

2.2 Plan of work:

The primary work is to synthesize the mesoporous Mg-Al-Ti composite oxide nanoparticles and check the adsorption capacity of arsenic from contaminated water. Then to improve the ceramic membrane's adsorption performance, synthesis of Mg-Al-Ti oxide nanoparticles incorporated MMM through sol-gel method such as In situ formed, polysulfone blend, and PVA coated ceramic membrane. Then the characterization of each MMM and at last comparing the characterization results of each membrane and selecting the best membrane for removing arsenic from drinking water as shown in **Figure 4**

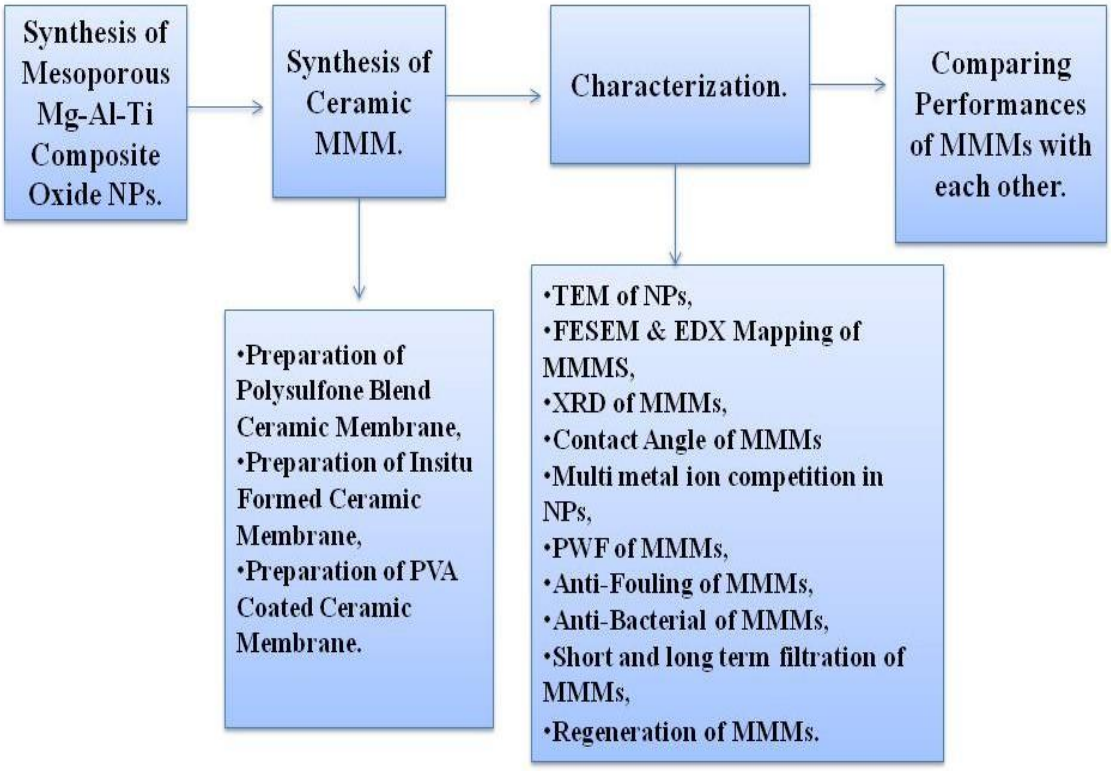


Figure 4. Flow chart of plan of work.



Figure 5. Ultra Filtration Unit

2.3 Process flow:

The experiments were done in an ultra-filtration unit **(Figure 5).** We can use both the retention and dead-end methods in this filtration unit. But for our experiments, we have selected the retention method, as in this method the larger molecules or the rejected heavy metals are brought back to the feed tank which results in no caking on the surface of the membrane. Hence, no clogging in the pores of the membrane, which eventually results in a longer lifespan of the membrane. The dead-end method is the opposite of the retention method. In this method, the rejected molecules and heavy metals remain on the surface of the membrane and develop cake on the surface of the membrane. Hence, clogging of the pores is relatively quicker.

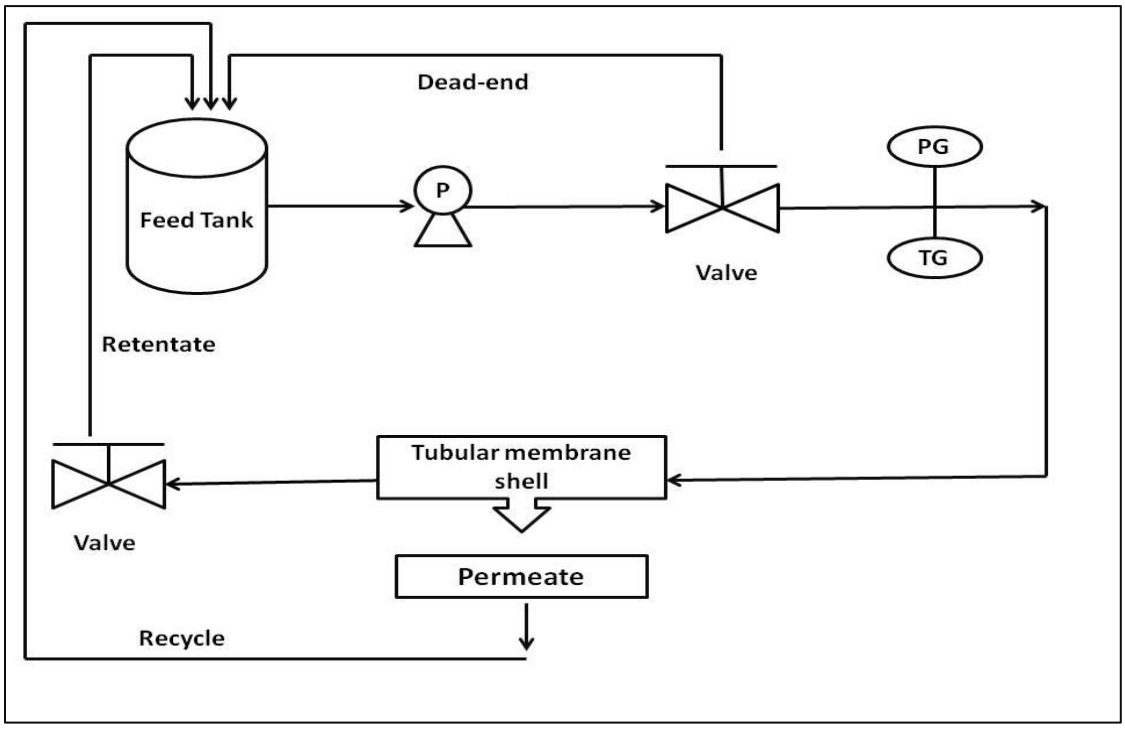


Figure 6. Process Flow of Filtration Unit.

2.4 Working principle of the unit

As shown in Figure (06) at first the tank is filled with contaminated water that is to be filtered. With the help of the RO pump the contaminated water passes through valve 1 with which retention and dead-end mode is selected. Once passed through the valve the contaminated water

is then filled in the feed spacer from the bottom of the tubular membrane shell at the desired pressure selected and maintained by valve 2. Then due to the electrostatic interaction of the contaminated water and the membrane, the adsorption occurs and the permeate is collected from the top of the tubular membrane shell and the rejected feed is then transported back into the feed tank.

Chapter 3

3. LITERATURE REVIEW

A literature review is a summary of previous research papers written on the same or similar topic of the research work that is to be done by us. It also provides the research gaps which is helpful information in research work. In this chapter, we have summarized the information collected from previous research papers which were helpful for us in writing this thesis. We have also mentioned the year of publication, the names of the previous research papers, and their respective authors. Citations have also been done to check the authenticity of the papers.

3.1 Heavy metal ions competition:

In 2022 Xiuzhen YangORCID, Haolin Zhang, Shuangchan Cheng and Bin Zhou studied the "Optimization of the adsorption and removal of Sb(III) by MIL-53(Fe)/GO using response surface methodology". In this study, a graphene oxide metal–organic framework (MIL-53(Fe)/GO) composite adsorbent was successfully synthesized using a simple method at room temperature. The specific surface area of the synthesized MIL-53(Fe)/GO nanoparticles was 268.43 $m^2 g^{-1}$, with an average pore size of 2.52 nm. The Box–Behnken response surface method was applied to optimize the adsorption time, dosage, pH, temperature, and initial concentration of Sb(III) in the MIL-53(Fe)/GO adsorption treatment employed for synthetic wastewater containing Sb(III). We determined the optimal adsorption conditions and explored the isotherm model, adsorption kinetic model, and adsorption mechanism during the adsorption process. For an optimal adsorption of Sb(III) by MIL-53(Fe)/GO, the adsorption time, dosage, pH, temperature, and initial Sb(III) concentration should be set to 4.86 h, 85.79 mgL^{-1}, 10.00, 39.29 °C, and 10.09 mgL^{-1}, respectively. Under these optimal conditions, the removal rate of Sb(III) will be as high as 97.97 %. The adsorption of Sb(III) by MIL-53(Fe)/GO conformed to the Freundlich isotherm adsorption model, and its maximum adsorption capacity was 69.014 mg g^{-1}. The adsorption kinetics process, which is a non-homogeneous reaction, could be fitted using a quasi-first-order kinetic model. A Fourier transform infrared spectroscopy analysis showed that MIL-53(Fe)/GO hydroxyl and amine groups play a vital role in the adsorption process. MIL-53(Fe)/GO did not exhibit any changes in its adsorption efficiency in the presence of its anion and showed high specificity to Sb(III). XPS characterization showed that Sb successfully adsorbed onto the adsorbent and that no oxidation–reduction reaction occurred during the adsorption process. The adsorption efficiency remained high even after four cycles of use. MIL-53(Fe)/GO is highly recyclable with significant application potential for treating wastewater containing Sb(III). [25]

In 2020 Xiaofeng Liu, Xin Xu, Xiaoqiang Dong and Jounboum Park studied the "Competitive Adsorption of Heavy Metal Ions from Aqueous Solutions onto Activated Carbon and Agricultural Waste Materials". In this paper batch adsorption experiments were conducted in single, and competitive systems. The adsorption efficiencies of different heavy metal ions were, in descending order: lead, copper, cadmium. Activated carbon showed best adsorption efficiency

(lead: 14.01 mg/g; copper: 13.1 mg/g; cadmium: 5.5 mg/g), followed by peanut shell (lead: 9.5 mg/g; copper: 49.1 mg/g; cadmium: 5.07 mg/g), and sawdust (lead: 5.5 mg/g; copper: 5.3 mg/g; cadmium: 3.99 mg/g), which showed the worst efficiency. The amount of heavy metal ions adsorbed onto activated carbon, peanut shell and sawdust increased with the increase of adsorption time and then reached equilibrium values. As the initial concentration of heavy metal ions increased, the amount of heavy metal ions adsorbed increased while the removal ratios thereof decreased. The adsorption processes in both single and competitive systems followed a Langmuir isotherm model and pseudo second-order kinetic model. The intraparticular diffusion process can be divided into two stages for the adsorption process of heavy metal ions. There were antagonistic effects among three kinds of heavy metal ions in a competitive system. [26]

3.2 Pure water flux:

In 2021 Akshatha R. Nadig, Nagaraj S. Naik, Mahesh Padaki, Ranjith K. Pai and Sébastien Déon studied on "Impact of graphitic carbon nitride nanosheets in mixed- matrix membranes for removal of heavy metals from water". In this study the prepared mixed matrix membranes showed enhanced performances towards water filtration. The incorporation of $g-C_3N_4$ into the membrane matrix caused an increase in the desired physicochemical properties like hydrophilicity and surface charge density. This in turn enhanced the rejection of heavy metal ions. The presence of free $–NH_2$ groups on the surface of the membrane helps in increasing the water permeability of the mixed matrix membranes. At 1 bar pressure, the mixed matrix membranes showed rejections higher than 95, 80, and 70 % for lead, cadmium, and arsenic, respectively. Anti-fouling properties of PSF membrane were also enhanced by $g-C_3N_4$, which was due to a notable increase in hydrophilicity and the formation of hydration layer on the membrane, preventing interactions between membrane surface and Bovine Serum Albumin (BSA). [27]

In 2022 Sahar Foorginezhad, Mohammad Mahdi Zerafat, Younes Mohammadi and Mohsen Asadnia studied "Fabrication of tubular ceramic membranes as low-cost adsorbent using natural clay for heavy metals removal". In this paper SnO_2/Montmorillonite nanocomposite is synthesized via the hydrothermal procedure and incorporated into the membrane matrix to decrease membrane fouling, enhance water flux, and improve heavy metals rejection rate. Results delineate 97.88–99.26 %, 76.79–92.23 %, and 24.97–64.74 % of Cu (II), Zn (II), and Ni

(II) removal from aqueous solutions in the 5–50 ppm range. An enhancement up to ~40% is observed upon nanocomposite incorporation. Furthermore, ~30 % increase in Cu (II) removal is obtained for SnO_2/ /MMT-incorporated membranes. [28]

3.3 pH testing

In 2021 Akshatha R. Nadig, Nagaraj S. Naik, Mahesh Padaki, Ranjith K. Pai and Sébastien Déon studied on "Impact of graphitic carbon nitride nanosheets in mixed- matrix membranes for removal of heavy metals from water". In this study the prepared mixed matrix membranes showed enhanced performances towards water filtration. The incorporation of $g-C_3N_4$ into the membrane matrix caused an increase in the desired physicochemical properties like hydrophilicity and surface charge density. This in turn enhanced the rejection of heavy metal ions. The presence of free – NH_2 groups on the surface of the membrane helps in increasing the water permeability of the mixed matrix membranes. At 1 bar pressure, the mixed matrix membranes showed rejections higher than 95, 80, and 70 % for lead, cadmium, and arsenic, respectively. Anti-fouling properties of PSF membrane were also enhanced by $g-C_3N_4$, which was due to a notable increase in hydrophilicity and the formation of hydration layer on the membrane, preventing interactions between membrane surface and Bovine Serum Albumin (BSA). [27]

In 2007 Wen-Bing Chu, Jia-Wei Yang, Ta-Jo Liu, Carlos Tiu and Jian Guo studied "The effects of pH, molecular weight and degree of hydrolysis of poly(vinyl alcohol) on slot die coating of PVA suspensions of TiO_2 and SiO_2". In the present study, a laboratory-scale slot die coating equipment was used to investigate the effects of pH, molecular weight and degree of hydrolysis of polyvinyl alcohol (PVA) on the coating window of PVA suspensions of TiO_2 and SiO_2. Measurements of steady shear viscosity, surface tension, and amount of PVA adsorption on particle surfaces of different suspensions, together with observations of coating bead by means of a flow visualization technique, were used to analyze the coating flow behavior. Changing the pH of the suspension affects both the surface tension and the amount of PVA adsorbed on the particle surface. While surface tension and degree of PVA adsorption were found to increase with increasing pH for the TiO_2suspensions, opposite effects were observed for the SiO_2 suspensions. The coating bead was found to be more stable for suspensions with higher values of surface tension and PVA adsorption, thus delaying the occurrence of air entrainment. Four

different PVA with varying molecular weight and degree of hydrolysis were used in the suspensions. Higher degrees of hydrolysis resulted in an increase in polymer adsorption, and hence larger surface tension. By contrast, higher molecular weight PVA resulted in a higher viscosity and a smaller surface tension, thus causing air entrainment to occur at a much lower maximum coating speed. [30]

3.4 Anti-fouling

In 2020 Chen Li, Wenjun Sun, Zedong Lu, Xiuwei Ao and Simiao Li studied the "Ceramic nanocomposite membranes and membrane fouling: A review". This paper mainly reviews the progress in the research and development of ceramic membranes, with key focus on porous ceramic membranes and nanomaterial-functionalized ceramic membranes for nanofiltration or catalysis. The current state of the available ceramic membranes in industry and academia, and their potential advantages, limitations and applications are reviewed. The last section of the review focuses on ceramic membrane fouling and the efforts towards ceramic membrane fouling mitigation. The advances in ceramic membrane technologies have rarely been widely reviewed before, therefore, this review could be served as a guide for the new entrants to the field, as well to the established researchers. [31]

In 2019 Chen Li, Wenjun Sun, Zedong Lu, Xiuwei Ao, Chao Yang and Simiao Li studied "Systematic evaluation of TiO_2-GO-modified ceramic membranes for water treatment: Retention properties and fouling mechanisms". In this paper the TiO_2-GO-modified ceramic membrane exhibited improved antifouling properties against HA and TA fouling. A modified Hermia's model was fit accurately to the experimental data obtained from long-term TA and HA fouling protocols for both pristine and modified membranes. The TA fouling mechanism transformed from a standard blocking to an intermediate blocking mechanism for the TiO_2-GO-modified membrane, indicating a dramatic decrease in the membrane pore size after modification. The gel layer formation model fit well for the modified ceramic membrane during HA filtration, which explained the decrease in the selected pharmaceutical retention by the HA-fouled membranes, while pore blocking governed the HA fouling for the pristine membranes, causing an increase in the pharmaceutical retention by the fouled membranes. The TiO_2-GO-modified membrane had a strong effect against bacterial adhesion, but only exhibited a minor inhibition of bio-fouling after a 24 h protocol in cross-flow filtration. [32]

In 2023 Xiaocan Zhang, Mengxin Wang, Pinglin Lin, Huixiao Ma, Yiran Liu, Ying Zhu and Qian Zhou studied the "L-Cysteine functionalized halloysite nanotubes/PVDF ultrafiltration membrane for improving anti-fouling performance". In this paper L-Cysteine is a hydrophilic zwitterionic amino acid, which contributes to the hydrophilicity and anti-fouling properties of the membrane. In this manuscript, an innovative nanocomposite (Cys-PDA-HNTs) was synthesized by spreading polydopamine on the outside of halloysite nanotubes (HNTs) as a secondary reaction platform and covalently grafting L-Cysteine by Michael addition reaction. A series of PVDF based ultrafiltration (UF) membranes were produced by mixing with different amounts of Cys-PDA-HNTs nanocomposite. XPS and FTIR were used to demonstrate the successful preparation of composite membranes, and their performance was characterized by WCA, water flux, BSA rejection ratio and anti-fouling measurements. It is found that M4 (with 1 wt % Cys-PDA-HNTs) had the greatest DI water flux (251.3 $Lm^{-2}h^{-1}$), lowest irreversible pollution ratio (18.5 %), highest flux recovery ratio (81.5 %) and the best long-term anti-protein fouling performance. This study offers a promising strategy to design novel UF membranes in the field of water purification. [33]

3.5 Long-term filtration

In 2024 Somakraj Banerjee, Aishwarya Das, Ranjana Das and Chiranjib Bhattacharjee studied "Mesoporous Mg–Al–Ti composite oxide incorporated mixed matrix ultrafiltration membrane with superior multi-heavy metal removal capacity, anti-fouling & anti-microbial property". In this paper with a maximum As(III) adsorption capacity of 256.6 mg/g, the membrane had a breakthrough volume of 25 L and could provide safe drinking water for 19 h from a real Arsenic (As) contaminated groundwater sample with a flux of 48 l/m^2-h. Beyond that, >90 % removal of Cd, Pb & Cr was also observed with maximum adsorption capacity of 652.9 mg/g, 332.5 mg/g, and 89.4 mg/g respectively. 92.5 % flux recovery after filtering a 1000 ppm bovine serum albumin showed the anti-fouling property. Successful inhibition of both gram-positive and gram-negative bacterial growth, and >99.99 % removal of colony forming units (CFU/ml) in the filtration process confirmed the anti-microbial resistance. With its multi functionality, these membranes hold great potential for practical water treatment applications. [35]

3.6 Regeneration

In 2016 Raka Mukherjee, Prasenjit Bhunia and Sirshendu De studied “Impact of graphene oxide on removal of heavy metals using mixed matrix membrane”. In this paper the graphene oxide (GO) impregnated mixed matrix membrane (MMM) was prepared by non-solvent induced phase inversion method. Efficacy of MMM for removal of heavy metals was explored using the developed MMM. It showed high adsorption capacity for Pb^{2+} (79 mg/g), Cu^{2+}(75 mg/g), Cd^{2+} (68 mg/g) and Cr^{6+} (154 mg/g) at natural pH, 6.7, 6.5, 6.4 and 3.5, respectively. The steady state permeate flux was around 30 l/m^2h for 50 mg/l feed concentration at 414 kPa transmembrane pressure drop and 40 l/h cross flow rate. Rejection of Pb, Cu, Cd, and Cr were in between 90% and 96 % for various operating conditions and the breakthrough time was around 10 h for different metal ions. The membrane was regenerated in-situ, by acidic solution at pH 5.5. [36]

3.7 Anti-bacterial

In 2023 Yuan He, Hai-Chuan Y, Ting-Ting You and Feng Xu studied “Sustainable and multifunctional cellulose-lignin films with excellent antibacterial and UV-shielding for active food packaging”. In this paper the natural biopolymers hold substantial prospects as food packaging materials due to the integrated advantages of excellent film-forming properties, biodegradability and appropriate mechanical properties. However, it remains a challenge to simultaneously endow antimicrobial, UV-shielding, water vapor and oxygen barrier properties of films. Herein, sustainable and multifunctional films were fabricated by constructing ε-polylysine (ε-PL) antimicrobial surface on the phenolated lignin/cellulose films (RCPL30). It is found that the fine control of electrostatic interactions and hydrogen bonding in anionic phenolated lignin/cellulose and cationic ε-PL is efficient for tailoring the structure and films performance. The addition of ε-PL effectively enhanced the antibacterial property, hydrophobicity, water vapor and oxygen barrier ability of the phenolated lignin/cellulose films. Antibacterial cellulose-lignin films with a high lignin content (30 %) were developed. In particular, the bactericidal rate reached almost 100% when the ε-PL concentration was 3% (LRCPL30-3). The water vapor permeability and oxygen permeability of LRCPL30-3 were as low as (3.21 ± 0.06) × 10−11 g m−1 s−1 Pa−1, (4.15 ± 0.13) × 10−16 cm3 cm/cm2 s Pa, respectively. Moreover, the phenolated lignin provided an exceptional UV shielding properties (100% for UVB and 99.91% for UVA for LRCPL30-3 sample) with high thermal stability and antioxidant activities. More importantly,

the as prepared LRCPL30-3 still showed high tensile strength (75.90 MPa). Based on these outstanding properties, LRCPL30-3 were used for shrimp package, which effectively extended shelf-life. Overall, the study highlights the benefits of biopolymers valorization and provides evidence of potential applicability of sustainable films (specially LRCPL30-3) as candidates for active food packaging. [39]

In 2023 Kongyan Li, Wei Zhong, Penghui Li, Jianpeng Ren, Kangjie Jiang and Wenjuan Wu studied "Antibacterial mechanism of lignin and lignin-based antimicrobial materials in different fields". In this paper it elucidates the antimicrobial mechanism of lignin, the factors influencing its efficacy, and the methods employed for its detection. Moreover, it describes the progress made in developing the antimicrobial capacity of lignin in different areas. In conclusion, this paper not only outlines the current state of research on the antimicrobial function of lignin, but also identifies challenges and future possibilities for enhancing its antimicrobial properties. This work holds great significance in the ongoing endeavor to contribute to high-impact research on natural alternatives for controlling infections and fostering environmentally conscious practices. [40]

In 2018 Michael J. Trimble, John T. Cheng, Quentin Vallé and Robert E.W. Hancock studied the "Critical Assessment of Methods to Quantify Biofilm Growth and Evaluate Antibiofilm Activity of Host Defence Peptides". In this paper biofilms are multicellular communities of bacteria that can adhere to virtually any surface. Bacterial biofilms are clinically relevant, as they are responsible for up to two-thirds of hospital acquired infections and contribute to chronic infections. Troublingly, the bacteria within a biofilm are adaptively resistant to antibiotic treatment and it can take up to 1000 times more antibiotic to kill cells within a biofilm when compared to planktonic bacterial cells. Identifying and optimizing compounds that specifically target bacteria growing in biofilms is required to address this growing concern and the reported antibiofilm activity of natural and synthetic host defence peptides has garnered significant interest. However, a standardized assay to assess the activity of antibiofilm agents has not been established. In the present work, we describe two simple assays that can assess the inhibitory and eradication capacities of peptides towards biofilms that are formed by both Gram-positive and negative bacteria. These assays are suitable for high-throughput workflows in 96-well microplates and they use crystal violet staining to quantify adhered biofilm biomass as well as

tetrazolium chloride dye to evaluate the metabolic activity of the biofilms. The effect of media composition on the readouts of these biofilm detection methods was assessed against two strains of Pseudomonas aeruginosa (PAO1 and PA14), as well as a methicillin resistant strain of Staphylococcus aureus. Our results demonstrate that media composition dramatically alters the staining patterns that were obtained with these dye-based methods, highlighting the importance of establishing appropriate biofilm growth conditions for each bacterial species to be evaluated. Confocal microscopy imaging of P. aeruginosa biofilms grown in flow cells revealed that this is likely due to altered biofilm architecture under specific growth conditions. The antibiofilm activity of several antibiotics and synthetic peptides were then evaluated under both inhibition and eradication conditions to illustrate the type of data that can be obtained using this experimental setup. [42]

In 2023 Mohammed Saleh, Zelal Isik, Pinar Belibagli, Hudaverdi Arslan, Serpil Gonca, Sadin Özdemir, Nurbolat Kudaibergenov, Alireza Khataee and Nadir Dizge studied “Fabrication of Ag nanoparticles coated leonardite basalt ceramic membrane with improved antimicrobial properties for DNA cleavage, E. coli removal and antibiofilm effects”. This study aimed to fabricate a novel, low-cost, and environmental-friendly ceramic membrane based on basalt and leonardite powders via press and sintering methods. The fabricated leonardite basalt ceramic membrane (LBCM) was coated with silver nanoparticles (AgNPs); to create an antibacterial surface. The capabilities of the bare and coated membranes were examined. In this context, water permeability reached 554 ± 2.61 and 447 ± 1.21 L/m2hbar for bare LBCM and AgNPs-coated LBCM, respectively. The fabricated membranes indicated 100% Escherichia coli (E. coli) removal efficiency at a transmembrane pressure of 0.5 bar. The solid surface antimicrobial activity of the LBCM and AgNPs-coated LBCM reached 26.38% and 100%, respectively. The LBCM and AgNPs-coated LBCM were analyzed for the in-vitro 2, 2- diphenyl-1-picrylhydrazyl (DPPH) antioxidant. Accordingly, AgNPs-coated LBCM exhibited higher antioxidant activities than raw LBCM. The scavenging capacity reached 83.91 % with AgNPs-coated LBCM, while only 58.95 % was achieved with raw LBCM, indicating that AgNPs-coated LBCM was better than bare LBCM from an antioxidant activities perspective. AgNPs-coated LBCM had a deoxyribonucleic acid (DNA) cleavage activity (single-strand DNA cleavage activity at 50 mg/L and double-strand DNA cleavage activity at 100 and 200 mg/L). In contrast, the raw LBCM did not exhibit DNA cleavage activity at any concentration. AgNPs-coated LBCM showed higher

antimicrobial activities (minimum inhibition concentrations (MICs) were 32 mg/L against Enterococcus faecalis (E. faecalis) and 64 mg/L against Staphylococcus aureus (S. aureus), Candida tropicalis (C. tropicalis), and Enterococcus hirae (E. hirae)). The biofilm inhibition of LBCM and AgNPs-coated LBCM powders was tested against S. aureus and Pseudomonas aeruginosa (P. aeruginosa). The maximum S. aureus inhabitations by LBCM and AgNP-coated LBCM were 60.34 % and 99.12 %, respectively. The inhabitation of P. aeruginosa increased from 52.38 % before coating to 96.37 % at the end of the coating process. Regarding E.coli microbial cell viability inhibition, LBCM powders and AgNPs-coated LBCM powders were found to inhibit E. coli growth by 68.35% and 100%, respectively. [43]

In 2024 Harleen Kaur, Merilin Rosenberg, Mati Kook, Dmytro Danilian, Vambola Kisand and Angela Ivask studied “Antibacterial activity of solid surfaces is critically dependent on relative humidity, inoculum volume, and organic soiling”. In this paper antimicrobial surface materials potentially prevent pathogen transfer from contaminated surfaces. Efficacy of such surfaces is assessed by standard methods using wet exposure conditions known to overestimate antimicrobial activity compared to dry exposure. Some dry test formats have been proposed but semi-dry exposure scenarios e.g. oral spray or water droplets exposed to ambient environment, are less studied. We aimed to determine the impact of environmental test conditions on antibacterial activity against the model species Escherichia coli and Staphylococcus aureus. Surfaces based on copper, silver, and quaternary ammonium with known or claimed antimicrobial properties were tested in conditions mimicking microdroplet spray or larger water droplets exposed to variable relative air humidity in the presence or absence of organic soiling. [44]

Chapter 4

4. MATERIALS & METHODS

In this section of the thesis, we discussed in detail about

4 Description of the materials used in the experiments,
5 Sources of the materials used,
6 Equipment used,
7 Experiments done,
8 Procedures of the experiments done,
9 How the study was conducted,
10 Procedures used to collect data,
11 Procedures used to analyze data.

4.1 Materials:

Polysulfone of average molecular weight 35 kDa, polyvinyl alchohol of molecular weight 360 kDa, precursors for adsorbent synthesis, aluminum isopropoxide (>98 wt %), titanium isopropoxide (97 %), magnesium nitrate hexahydrate ($Mg(NO_3)_2.6H_2O$), and the soft template Pluronic P123 (Mn = 5800, $EO_{20}PO_{70}EO_{20}$, EO = Ethylene oxide, PO = Propylene oxide) was purchased from Sigma-Aldrich. Arsenic salt $NaAsO_2$ was purchased from Loba Chemie Pvt. Ltd. Solvent N, N-Dimethylacetamide (DMAC, 99.5 %), KCl, Na_2HPO_4, KH_2PO_4, C_3H_8O, $C_5H_8O_2$, HNO_3 (about 70 % w/w), NaOH, $NaNO_3$, NaCl, NaOCL, $Pb(NO_3)_2$, $Cd(NO_3)_2$, $K_2Cr_2O_7$, crystal violet was obtained from Merck. Albumin Bovine fraction V powder (pH 6.0 to 7.0) was purchased from Sisco Research Laboratories Pvt. Ltd. Ceramic membrane was purchased from Need Inovation. The bacterial stock cultures stock cultures, Escherichia coli-NCIM 2065, Pseudomonas aeruginosa NCIM-2037, Bacillus subtilis NCIM 2655, and Staphylococcus aureus NCIM-2679 were purchased from NCIM, Pune. Chemical reagents were used without any purification or treatment. Deionized water from Sartorius Arium Pro was used for synthesis and other experiments.

4.2 Methods4.2.1 Synthesis of mesoporous Mg–Al–Ti composite oxide nanoparticles:

At first, in a batch synthesis, we dissolved 2.5 g P123 in 50 ml ethanol at room temperature. Then 20 mmol of three metal oxide precursors (Mg, Al, Ti precursors in 3:1:1 ratio) were added to the solution with 4 ml HNO_3 (70 % w/w). To create a homogeneous mixture the blend was covered and agitated for 5 h. After that, we kept the mixture in a hot air oven at 60° C for 48 h for solvent evaporation. After 48 h a white-yellowish solid was obtained. The resultant material underwent two stages of heating in a muffle furnace; a ramp rate of 1° C/min up to 200° C and an increased ramp rate of 10° C/min up to 400° C were used and then kept under that temperature for 4 h. White flakes found after calcination were ground to obtain fine powdered NPs.

4.2.2. Synthesis of MMMs:

Ceramic membranes have high mechanical, thermal, and chemical strength and to improve the separation performance we have applied different types of coatings on the ceramic membrane. MMM has a range of nanofillers like impermeable fillers (nanoparticles) and permeable fillers (nanoparticles). It is a challenge to create a dispersion of mixed matrix membranes by combining the properties of both nanofillers and polymeric membranes. We have been working on improving the ceramic membrane properties by exposing it to different types of nanoparticles and synthesizing a thin film of nanoparticle-incorporated polymers like polysulfone and PVA. A lot of research has been done on PVA membrane development and the main reason behind it is that it is a cheap material, has excellent film-forming properties, and can be synthesized in aqueous form which is a green manufacturing process. But its drawback is that it is very unstable in water, to be precise it swells in the water and loses its selectivity. Hence, to overcome this problem, we used the sol-gel method by adding some cross-linking agents like glutaraldehyde and HCl. This is how we achieved organic, and inorganic bonding and uniform dispersion of nanoparticles in PVA. The same method has been followed to prepare polysulfone blend membranes. The image of prepared MMMs is shown in **Figure (07).**

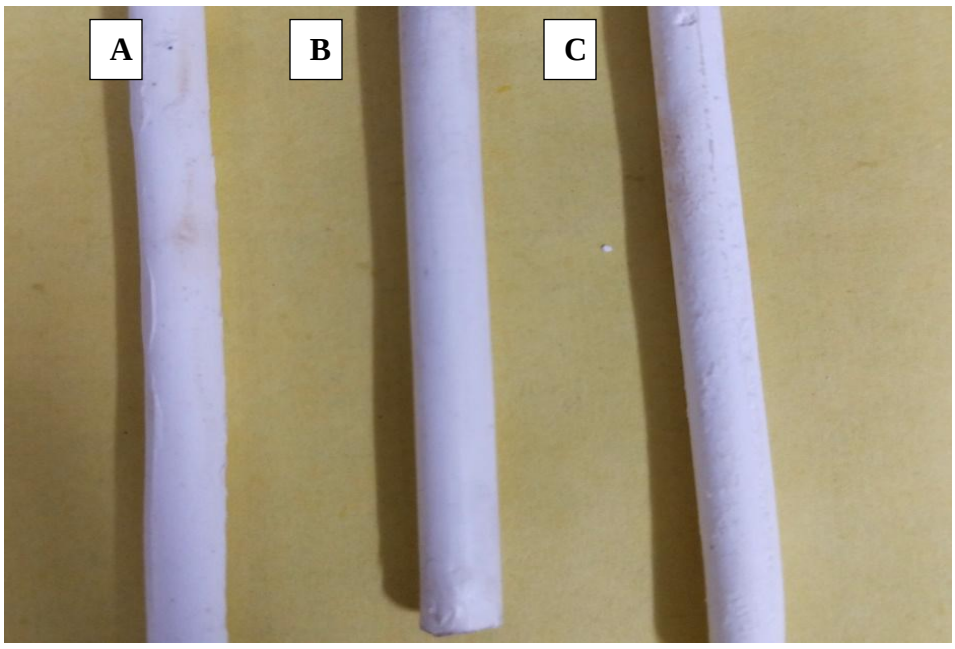


Figure 7. Image of prepared mixed matix membrane A. PVA Membrane, B. PSF Membrane, C. In-situ Membrane.

4.2.2.1 Preparation of Polysulfone blend Ceramic Membrane:

A polymer layer was synthesized on the ceramic support by the non-aqueous sol-gel method. At first, we prepared a binding solution by dissolving 17 % polysulfone, 3 % P123, 0.8 % nanoparticles, and 79.2 % DMAC (N, N, Dimethyl Acetamide) in a beaker by a magnetic stirrer. After vigorous stirring for an hour or until a homogeneous solution was achieved, we dipped the ceramic membrane in the prepared solution. Once a layer of polymer was formed on the membrane, the coated membrane was placed in a petri dish to submerge it into cold deionized water. Then the membrane was kept in the refrigerator for 24 hours to set the polymeric layer on the surface of the ceramic membrane and then the membrane was aired dried.

4.2.2.2 Preparation of In-situ Formed Ceramic Membrane:

A solution was prepared with 2g P123 in 40 ml abs. ethanol. Then with 3.2 ml HNO_3 (70 % w/w) three metal oxides which are 12 mmol Mg (NO_3). $6H_2O$, 4 mmol Al Isopropoxide, and 4 mmol Ti Isopropoxide were mixed in the solution. These chemicals were stirred on a magnetic stirrer for 4 hours or until a homogeneous solution was achieved. Once a homogeneous solution was formed, the ceramic membrane was dipped in the prepared solution and was then kept in the temperature controller at 60º C for 2 days. After that the temperature was set at 200º C in a muffle furnace and the membrane was kept in it for as much time as required to reach 200º C, when the temperature is rising at 1º C/minute. Then the membrane was kept in a muffle furnace at 400º C for 4 hours.

4.2.2.3 Preparation of PVA Coated Ceramic Membrane:

A solution was prepared with 5 % PVA with 50 ml water and 0.5 % NPs on heating magnetic stirrer at 90º C. The PVA and NPs were added gradually while stirring the solution. Once a homogeneous solution was formed then the temperature was turned off and the solution was cooled down to room temperature to add 2 % glutaraldehyde and 0.5 % HCL to the homogeneous solution. After the addition, the solution was stirred for an hour without heat, then the solution was ultrasonicated for 10 minutes, then it was again cooled down to room temperature. Once cooled down, the ceramic membrane was dipped in the solution and was kept for air drying for 24 hours. At last, the coated, air-dried ceramic membrane was kept in a muffle furnace at 110º C for 1 hour.

4.3 Characterization

4.3.1 TEM Analysis :

Morphology and nanostructures of Mg–Al–Ti composite oxide nanoparticles were investigated through transmission electron microscope (TEM) imaging. **Fig (8)** shows the schematics diagram of a modern TEM. An electron gun generates electron beams, which is closely focused by metal apertures and electromagnetic lens in the column of a TEM. The electrons behave as negatively charged particles, then the electrons are deflected by magnetic or electric fields. In this process, electrons that are in small energy range can pass through which leads to a well-defined energy electron beam. Then, the transmitted electrons are applied on the sample which was placed on the sample holder in the column of a TEM. The thickness of a TEM specimen should be within 100 nm for electrons to pass through. If the specimen is porous then more electrons will pass through it and less electrons will pass through dense materials The transmitted electrons are refocused and then magnified by an electromagnetic lens system consisting of two lenses after that they pass through the specimen, and are projected on a phosphor screen to convert the electron image information to a visible form. In the entire imaging system, the emitting directions of electrons could be changed with electromagnetic lens such as condenser, objective, and projective lens. It should be noted that the phosphorescent plate glows when being hit by electrons during the TEM imaging process. The entire imaging system of a TEM is also similar to photography [14].

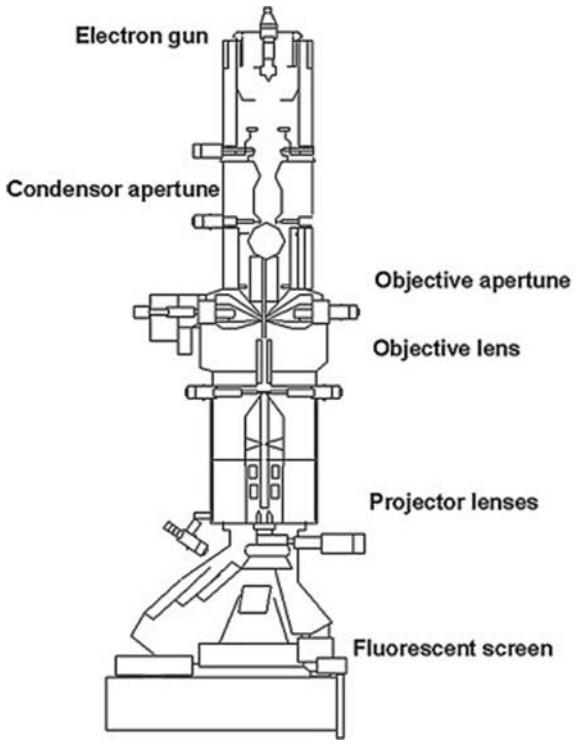


Figure 8. Schematic diagram of a modern TEM [14].

4.3.2 XPS Analysis:

XPS stand for X-ray photoelectron spectroscopy, it is one of the standard tools used for the characterization of material surface. It works on the principle of photoelectric effect by which it can identify the elemental composition of a material. It is a surface sensitive technology which typically analyzes a material to a depth of 5 nm. When electromagnetic radiation such as x-rays is made incident on the sample surface, they penetrate into the sample surface. The core electron of the atom absorb the x-ray photon energy and if the incident photon energy high enough then this core electrons knocked off the atom. This ejected electrons are called photoelectrons. The kinetic energy of the ejected electron is the characteristic of the atom from which these electrons are coming out. Therefore, by measuring the kinetic energy of these electrons, we can identify the atom. We can also identify from which orbit the electron is coming out.

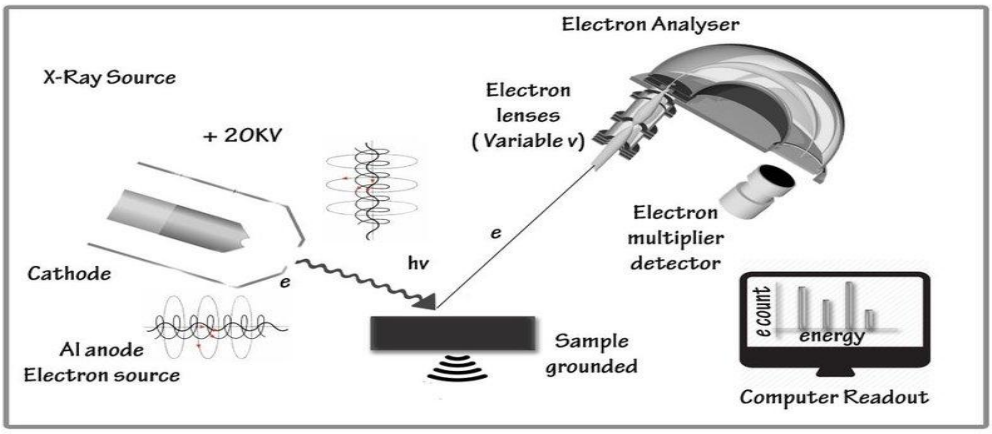


Figure 9. Schematic diagram of XPS [15]

The schematic of XPS is shown in **Figure (09)** here we can see a sample holder on which the sample is kept, x-ray coming out of x-ray tube are made incident on the sample surface. These x-rays penetrate into the atoms of the sample surface then the core electrons of the atom absorbs the x-ray photon energy and if the photon energy is high enough then these electrons are ejected from the atom. Then the energy is measured with the help of electron energy analyzer and their number is counted with the help of electron detector. After that the information is provided to the computer system and then it plots the graph of intensity of electron vs energy, the graph is called as XPS spectra. With the help of XPS spectra, the elements present on the sample surface can be identified. XPS spectra is a count of electrons versus kinetic energy of electron, the kinetic energy can be converted into binding energy with the help of **Eq.1**

$$h\nu = BE + KE + \Phi \qquad \textbf{Eq.1}$$

where hv is energy of the incident photon and Φ is the work function that mean the energy required to knock off the electron from the atoms, KE is kinetic energy and BE is binding energy. So if convert kinetic energy into binding energy the formula will be from **Eq.2**

$$BE = h\nu - (KE + \Phi) \qquad \textbf{Eq.2}$$

From this relation we can note that lower the kinetic energy means higher the binding energy and higher the kinetic energy means lower the binding energy. Therefore, if a graph of count of

electron vs binding energy is plotted then binding energy will decrease as we move from left to right. Now, the binding energy of electron moving in a particular orbit of atom of particular element are already known to us. Binding energy indicated by the peaks in graph, we can compare with the non-binding energies of the electrons moving in a particular orbit of an atom of a particular element. By comparing these energies we can identify the atoms of which element are present on the sample surface [15].

4.3.3 BET Analysis:

If we have porous sample with pores of different sizes on the top surface, during analysis we degas the sample to ensure that it's totally clean. Then we dose a gas at a series of pressures which will absorb to the surface and to the walls of the pores. At this stage, the sample including the walls of the pores are covered in a layer of adsorbate just one atom thick is called the monolayer and given the volume of the monolayer is the fairly straight forward calculation to convert to the area covered by it, in other words the surface area of the sample [16]. So, we start with a clean flat surface without any pores or surface roughness and if we introduce our analysis gas (the adsorbate) to the sample below atmospheric pressure. We immediately have adsorbate atoms in the gaseous phase above the sample, the atoms in the gaseous phase will as they move about land on the solid surface and when they do they may just rebound straight back into the gaseous phase or for short period of time, they may remain on the surface in which case we say they have adsorbed to the surface. The adsorption is due to an interaction of attractive forces between the gaseous phase adsorbate and the solid surface. These attractions are very weak such as van der waals forces. So, the adsorption is refer as physisorption or physical adsorption. The enthalpy of adsorption is quite low, certainly less than 50 kilojoules per mole. Once it's all done, a term will tend to resident on the solid surface for a short period of time before being dislodged and return into gaseous phase. Now, this might be caused by the constantly moving solid surface or it may be struck by another atom from the gaseous phase. Atoms will tend to move between the phases but any adsorption pressure a dynamic equilibrium will established over time between atoms in each of the phases. For surface area measurement we are ultimately attempting to achieve the monolayer adsorption. Whereby the equilibrium between gaseous and adsorbed phases involves the solid surface being covered in a complete layer of adsorbate just a single atom thick. It's the formation of this state that is assumed in the Langmuir model and that's one

of the earliest approaches to adsorption. But the adsorption of a distance monolayer actually forming during physisorption is most likely to be wrong and the application of the Langmuir modal to the calculation of surface area is rather limited in this respect. In reality multilayer adsorption may also be occurring, the samples will almost certainly have surface roughness, pores of range of shapes and sizes and also the presences of charged surfaces species [16]. The most common adsorbate is nitrogen, now that's diatomic, non spherical and has quadrupole moment. This will lead to surface science become preferentially non equivalent adsorbate. The measurement of the monolayer adsorption for the occurrence of multi-layer adsorption is recognized and accounted for in BET theory, named after its creators brunel, Emmett and Teller. This gives the BET equation **(Eq.3)** for monolayer adsorption volume [17]

$$\frac{\frac{P}{PO}}{n\left(1-\frac{P}{PO}\right)} = \frac{1}{n_m C} + \frac{C-1}{n_m C}\left(\frac{P}{PO}\right) \qquad \textbf{Eq.3}$$

Where at a specific relative pressure (P/PO), n is the quantity of adsorbate adsorbed, nm is the monolayer capacity, C is the BET C-value. **Eq. 4** is for BET surface area is

$$SBET = \frac{n_m . L . \sigma_m}{V_o . m} \qquad \textbf{Eq.4}$$

Where L is the Avogadro constant, σm is the molecular cross sectional area of the adsorptive (0.162 nm2 for N2), m is the sample mass, Vo is the molar gas volume of the adsorptive at STP [17]. The **Eq.5** is to find BET C value is

$$C \propto e^{\frac{q1-ql}{RT}} \qquad \textbf{Eq.5}$$

Where q1 is the heat of adsorption of the first adsorbed layer, ql is the heat of liquefaction of the adsorbate, R is the gas constant, T is the temperature [17].

4.3.4 FESEM Analysis:

Morphology of our samples, the MMMs was probed by a FESEM (model: Inspect F50, FEI). **Figure (10)** is the schematics diagram of the field emission scanning electron microscope (FESEM). It is a type of electron microscope that images the sample surface by scanning it with a high-energy beam of electrons in a raster scan pattern. Electron emitters from field emission gun was used. These types of electron emitters can produce up to 1000X the emission of a

tungsten filament. However, they required much higher vacuum conditions. After the electrons beam exit the electron gun, they then confined and focused into a thin focused, monochromatic beam using metal apertures and magnetic lenses. Finally, Detectors of each type of electrons are placed in the microscopes that collect signals to produce an image of the specimen [18].

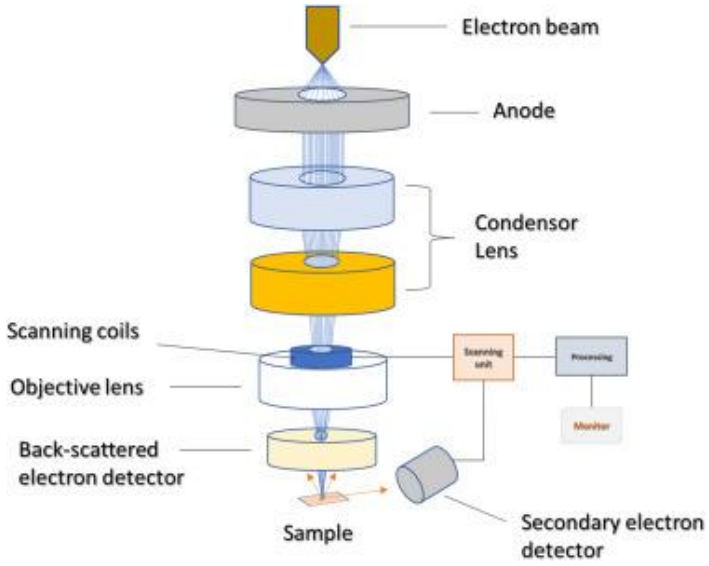


Figure 10. Schematic diagram of FESEM [19]

4.3.5 XRD Analysis:

Figure (11) shows the diagram of working principle of XRD. It is a powerful characterization technique which is used to check the material crystallinity. If we get shape peaks, it means that the material is crystalline in structure. Hence, there is a periodicity of atoms in the material. Periodicity of atoms in the material defines the height of the peak. More periodicity higher the peak, less periodicity lower the peak [20]. This happens due to the diffraction, higher the electron density variation, higher the intensity for the plane reflected in the XRD pattern. And if we get broad peaks, it means that the material is amorphous. It is due the disorderness of atoms in the material. If we look closely to the peaks, the peaks have some or more width. Peak width is a function of crystallinity, good crystallinity means less broader peak. Residual stress in material also affects the width size of the peak. More the stress or strain with the material, broader the

peak will be. Crystallite size can also be calculated with the broadness of the peak. Smaller the crystallite size broader the peak. Formula to calculate crystallite size is given in **Eq.6**

$$\beta = \frac{K\lambda}{L\cos\theta} \qquad \textbf{Eq.6}$$

In an x-ray diffraction analysis, a sample is placed into the center of an instrument and illuminated with a beam of x-rays. The x-ray tube and detector move in a synchronized motion the signal coming from the sample is recorded and graphed where peaks are observed related to the atomic structure of the sample [20]. The relationship between the diffraction angle and the spacing between the atoms can be determined by applying the sine function **(Eq.7)**

$$\textbf{Sin}\theta = (\lambda/2)/d \qquad \textbf{Eq.7}$$

Rearranging this equation yields an equation commonly known as "Bragg's Law" **(Eq.8)**

$$n\lambda = 2d\sin\theta \qquad \textbf{Eq.8}$$

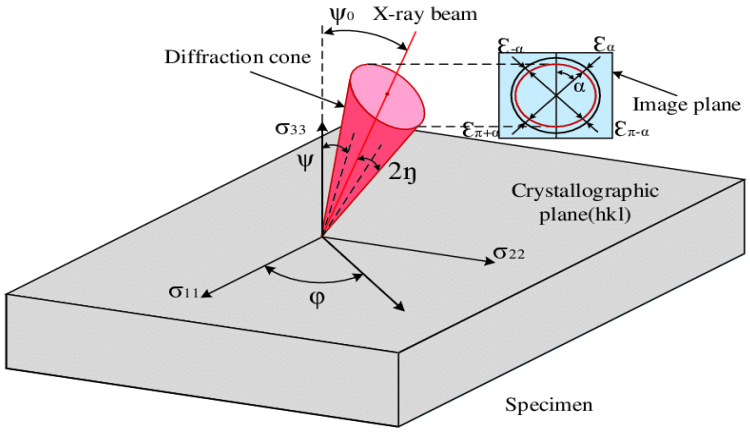


Figure 11. Schematic diagram of XRD [21]

4.3.6 Contact Angle:

The contact angles of the MMMs were measured by the sessile drop method at room temperature using a goniometer (model: Apex instruments, ACAMNSC 30). The contact angle test is done to know the surface-wetting properties of the membrane. It plays an important role in membrane properties and performances during the separation process such as permeate flux, rejection, and fouling characteristics. The factors like pH, temperature, charge density, and surface energy can also affect the interaction of membrane surfaces [22]. In the case of perfect wetting, we have theta that is equal to 0° whereas in the case of perfect non wetting theta is 180°. But in most cases, we have something in between two where theta is between 0 and 180°. Hence, 90° is the angle that determines that the material is wetting or non-wetting, if the contact angle is below 90° then it is considered that the material is hydrophilic/wetting in nature, and if the contact angle is greater than 90° then the material is hydrophobic/non-wetting. If the contact angle is close to the theoretical limit of 180° then the surface is considered as super-hydrophobic. Hydrophilic means the tendency of the surface to wet or forming a thin hydration film over the surface (water-loving). The non-wetting characteristic of the surface or showing less affinity toward the liquid, such surfaces are called hydrophobic. Due to surface tension water or any other liquid forms a spherical shape, it is because water molecules within the liquid are attracted to each other. These water molecules can form h-bonding with other water molecules around them. So the fact that water and other liquid molecules are attracted to each other is known as cohesion and this attraction force is called cohesion force. Since these water molecules like to bunch together or form groups, but due to cohesive force, a molecule is pulled equally in all directions by neighboring molecules. This results in a net force of zero. However, at the surface, there is no water molecule above them. These are less restricted and are in a state of higher energy compared to the molecules in the bulk of the liquid. This allows surface water molecules to group a little better and form stronger, tighter bonds, in such a way that they form a tension that is not present in the water molecules below the surface. These bulk water molecules will prevent surface molecules from grouping by pulling the molecules toward the center. Since the force is only downward and sidewise, the liquid forms a spherical shape [22]. So, surface tension is the tendency of a liquid surface to shrink into the minimum surface area possible because liquid molecules can make or maintain a spherical shape. High surface tension liquid will form a high contact angle and will stay in a spherical droplet, whereas a low surface tension liquid will

have a low contact angle compared to high surface tension liquid and will show the tendency of wetting which means this will spread out on the solid surface. Fundamentally, contact angles are a function of the interaction of the surface tension involved. There are three boundaries to consider when a droplet is in contact with a solid surface. The solid, the liquid, and the vapor surrounding them which is usually air. We have the surface tension of liquid against vapor, the surface tension of solid against vapor, and surface tension of liquid against solid. The contact angles can be calculated by Young's Equation [22].

4.3.7 ICP-OES:

ICP-OES stands for Inductively Coupled Plasma Optical Emission Spectroscopy. It is a technique to identify the type and amount of water dissolved compositions of elements by measuring the characteristics of their wavelengths using plasma and spectrometer.

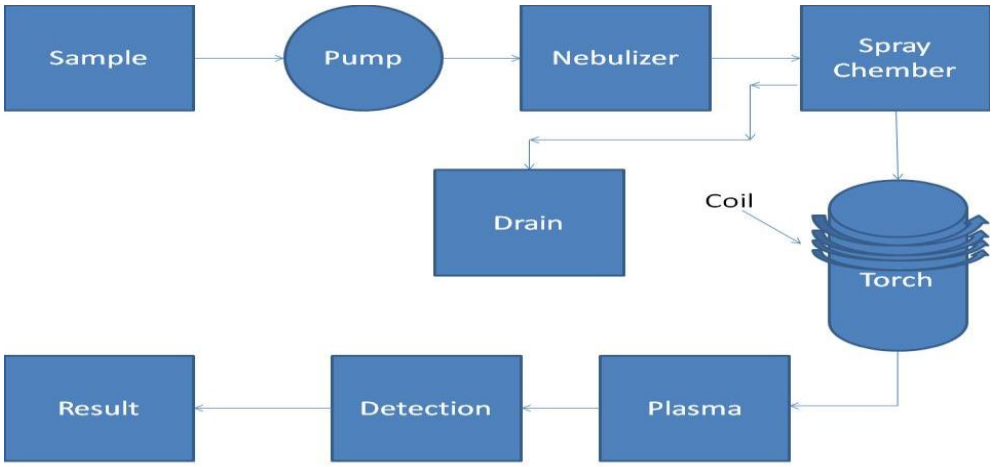


Figure 12. Diagram of ICP-OES.

The above image **Figure (12)** shows the working process of ICP-OES. At first run 2 or 3 % diluted HNO_3 solution to clean the system. Then the liquid sample is drawn into the peristaltic pump. The pump sends the liquid sample to the nebulizer where the liquid samples are converted into fine aerosols [23]. Then in the spray chamber, large droplets are drained away and the finer droplets are directed into the hot argon plasma. The plasma is generated at the end of a quart torch by a cooled induction coil through which a high-frequency alternate current flows. The temperature of plasma ranges between 6000-7000 K and sometimes 1000 K. In the plasma, the sample aerosols vaporize, and due to the thermic energy, the ions and the atoms of the samples

get excited [23]. So that their characteristic wavelengths of light can be emitted. Then the light is transferred into a high resolution no-purge sealed optical system, which separates the light into specific wavelengths for the elements to be measured. As the wavelengths strike the detector array, the intensity of light for each different wavelength is qualified. A sophisticated software converts the intensity of lights into concentration units. Then the given sample contains which element in what amount is revealed [23].

4.3.8 UV Visible Spectroscopy:

Spectroscopy is the study of the interaction between electromagnetic radiation and matter. Any biological molecule, protein, DNA, RNA, or any chemical compound can be studied. EMR are the waves that show the properties of both electric and magnetic like gamma rays, x-rays, and uv rays. The EMR used in UV-visible spectroscopy is UV visible light and we can take any matter for study. As UV visible light is used in this spectroscopy that's why it is called UV visible spectroscopy. If we arrange the EMR waves based on wavelength, we get an electromagnetic spectrum. In this spectrum, the gamma rays are arranged first, the longest wavelength is the radio wave which comes last. Due to short wavelength, the gamma rays have high energy and the radio waves have less energy [24].

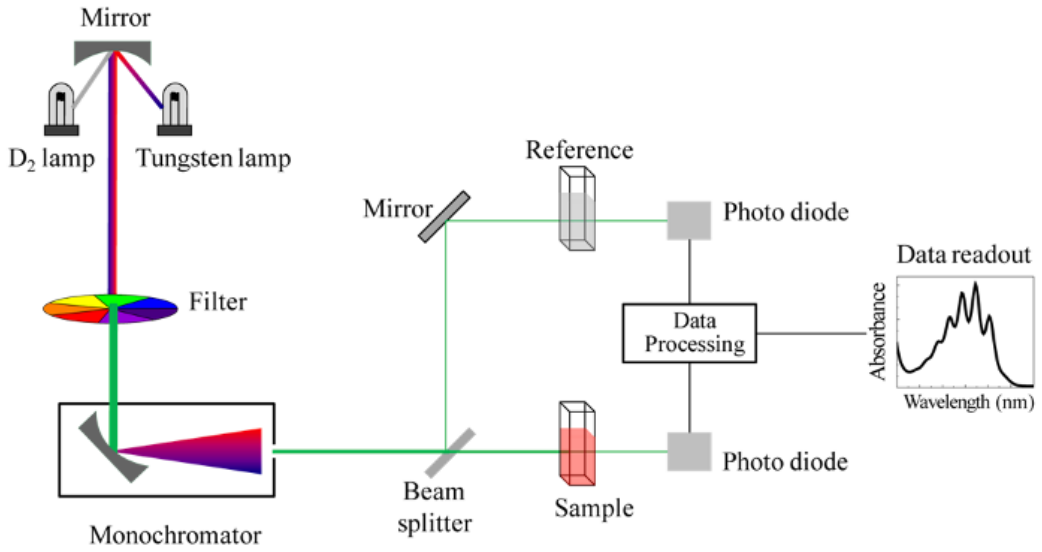


Figure 13. Schematic diagram of UV-Visible Spectroscopy [24].

In UV visible spectroscopy instrumentation **Figure (13),** first comes a lamp, which produces a wavelength of 200 to 800 nanometers. The wavelength of 200 to 800 nm is the wavelength of UV visible light. Specifically, the wavelength of UV light is 200 to 400 nm and the wavelength of visible light is 400 to 800 nm. Monochromator is made up of two slits and a prism. The first slit role is to make the photon particles of the light produced by the monochromator fall parallel to the prism. So that all the light falls parallel to the prism. Then the prism separates the light from the prism into different wavelengths. After that, a specific wavelength of light passes through the second slit. The light of the second wavelength is converted into two rays of equal intensity. The first ray of the light goes to the reference cell. A reference cell is a cuvette made up of glass or quartz, the sample is kept in the open side of the glass or quartz. In the reference cell of the cuvette, only the buffer solution or blank sample is taken. Whatever intensity of the first ray of light falls on the buffer solution passes through it as it is, because there is no sample solution in the buffer solution, there will be no absorption. The second ray of light falls on the cuvette which has a sample solution to be read. For example, if we take a protein then the protein will absorb the light falling on it and after the absorption as the protein is made up of amino acids, amino acids will have a double bond and a ring structure. These amino acids use the energy for electronic transition, the electrons of the amino acids move from the lower energy state to the higher energy state by absorbing the light energy [24]. This results in the light passing through the cuvette having less intensity. The absorption depends on two factors, if the concentration of the protein is high then the absorption will be high. The length of the cuvette is called the path length, if the path length is high then also the absorption will be high. The concentration and path length of the protein are shown by the Beer- Lambert law, beer states that if the concentration is high then the absorption will be high and Lambert states that if the path length is high then the absorption will be high. According to this law **(Eq.9)**

$$A \propto CL \qquad \textbf{Eq.9}$$

The less-intensity light transmitted from the protein cuvette and the high-intensity light transmitted from the reference cell is then detected by detector. The detector detects the ratio of transmitted light and sends the reading to the recorder. The recorder generates a reading in the form of absorbency. The reading is interpreted to find the absorption and concentration of the protein [24].

4.3.9 Heavy Metal Ions Competition:

Actual wastewater is complex in terms of its composition. There are multiple anions and different heavy metal cations. Because the adsorption process will compete with the target pollutants to be removed, the existence of coexisting ions is another important factor affecting the actual removal capacity in practice [25]. Competition between heavy metal ions affects the adsorption efficiency of every ion. The adsorption sites of the adsorbent will be replaced by other heavy metal ions in a competitive system, thus the adsorption capacity of the same heavy metal ion decreases in a competitive system [26]. Here, we have investigated the adsorption capacity of four different heavy metals (Cd, Cr, As, and Pb) with each other. The adsorbent mesoporous Mg–Al–Ti composite oxide nanoparticles were in equal quantity (10 mg) for different concentrations (20 ppm, 10 ppm, and 1 ppm) of adsorbate. The adsorbent and adsorbate of all concentrations were vigorously stirred overnight. Then permeate was filtered out with the help of filter paper and was tested in ICP-OES. **Figure (14)** shows the drastic color change, with this image we can see the difference in the color shades of the feed and the adsorbed permeates of different concentrations.

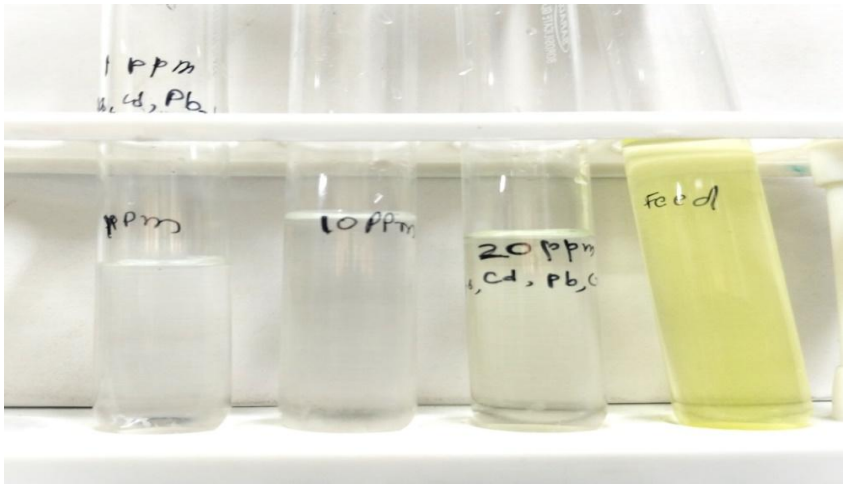


Figure 14. Multi metal Adsorption.

4.3.10 Pure Water Flux:

A pure water flux experiment was carried out at room temperature using a retention filtration unit with a feed tank capacity of 1500 ml. Water flux describes the amount of permeate collected during membrane separation. The PWF of the membranes was measured by passing DI water

through the membrane at different trans-membrane pressures ranging between 30-200 psi in a retention setup [27]. The water flux is measured using the relationship between volume, area, and time shown in **Eq.10** :

$$\mathbf{J_w = Q\ A.\Delta t} \qquad \textbf{Eq.10}$$

Where,

J_w =pure water flux ($\frac{L}{m^2}.hr$)

Q = amount of water collected (L)

Δt = time interval(hr)

A = the membrane area (m^2)

To investigate the membrane performance as a function of filtration time and water flux. A pure water filtration test was performed at different time intervals. The filtration test was carried out of the 1 ppm feed at various pressures. Once, the permeate reached its equilibrium at a particular volume, the permeate water was collected to calculate the water flux at each pressure [28].

4.3.11 pH Testing:

To investigate the arsenic removal or rejection percentage at different pH levels. The pH of an aqueous solution of arsenic was adjusted to the desired level using either HCL acid or NaOH [29]. The desired pH ranges were between 3-13 pH which was measured by using a pH meter [27, 30]. The feed was then run in the filtration unit at a constant pressure and permeates of different pH were collected. The adsorption of collected permeates of different pH was tested in ICP. Then the removal percentage was calculated using **Equation 11**:

$$\textbf{Removal}\ \% = \frac{\textbf{Feed} - \textbf{Permeate}}{\textbf{Feed}} \times \mathbf{100}\% \qquad \textbf{Eq.11}$$

4.3.12 Anti-Fouling:

Fouling is one of the major drawbacks of ultra-filtration membranes, it degrades the membrane performance decreases the membrane life span, and increases its maintenance cost [31, 32]. Hence, it is necessary to check the anti-fouling properties of the membrane before industrial

application. To measure the anti-fouling property of our three developed MMMs, the antifouling test was conducted. A protein solution of bovine serum albumin (BSA) was used to study the antifouling property of the control and the best-performed membrane. At first, the feed solution of DI water was run in the filtration unit and the pure water flux of a particular membrane was calculated which was denoted as J_1. Then a 1000 ppm solution of BSA was run in the filtration for the fouling of the membrane. The water flux of the BSA solution permeate was also measured, denoted as J_p. All the studies were conducted at a constant pressure of 1 bar. Once, the BSA water flux was measured, the membranes were washed with warm DI water and the tank was cleaned with C_3H_8O [33]. The warm DI water was run as feed for an hour at low pressure to remove the BSA adsorbed from the surface and the pores of the membranes. After the reversible fouling the water flux of the cleaned membrane was measured and it was denoted as J_2 [34]. To analyze the anti-fouling property in detail the following **Eq.12, 13, 14, and 15** were used for the calculation

$$\mathbf{FRR\ (\%) = \frac{J_2}{J_1} \times 100} \qquad \textbf{Eq.12}$$

$$\mathbf{R_r = \left(\frac{J_2 - J_p}{J_1}\right) \times 100} \qquad \textbf{Eq.13}$$

$$\mathbf{R_{ir}\ (\%) = \left(\frac{J_1 - J_2}{J_1}\right) \times 100} \qquad \textbf{Eq.14}$$

$$\mathbf{R_t(\%) = \left(1 - \frac{J_p}{J_1}\right) \times 100} \qquad \textbf{Eq.15}$$

R_t, R_{ir}, R_r, and FRR, characterize the overall anti-fouling performance of the membranes. R_{ir} is the percentage of irreversible fouling which occurs as a result of the strong interaction between the foulants and membrane surface due to the pore blocking by the foulant. R_r is the amount of reversible fouling for which the foulants are reversibly bound to the membrane surface but can be removed by washing with warm water. The various reasons for membrane fouling are electrostatic force, hydrogen bonding, hydrophobic, and Van der Waals forces. The fouling mechanism is mainly dominated by hydrophobic interaction between the membrane surface and BSA. Hydrophilicity plays a major role in presenting resistance against the fouling by creating a layer of hydration on the membrane surface inhibiting the interaction of BSA and the membrane surface [27].

4.3.13 Long-Term Filtration :

The long-time filtration experiment of 100 ppb total As solution, was performed to find out the membranes during a breakthrough volume of the MMMs. Breakthrough volume denotes the exhaustion of the continuous operation [35]. A feed of 100 ppb As the solution was 1000 ml in volume. We ran the feed at a constant 1 bar pressure until the total 1000 ml volume of permeate was recovered. The collected permeate was then tested in ICP to know the concentration of the total permeate. If the concentration was below 10 ppb (permissible As limit) then 2nd batch of 100 ppb feed was run. If the total permeate was not below 10 ppb then it was again run as feed until the permeate concentration reached below 10 ppb. This experiment tells the amount of water a membrane can filter out.

4.3.14 Regeneration :

The regeneration performance of spent membranes is an important indicator that can help evaluate their economic aspects in practical applications. For prolonged usage, the spent membranes were regenerated by achieving desorption of heavy metal ions from it, In-situ chemical regeneration was used. The MMMs with adsorbed As salts were regenerated in an acidic solution [36]. The membrane was first thoroughly washed with distilled water, then 1 liter of acidic solutions of 0.1N NaOH was filtered out until the increase in flux became constant and then HCl was passed through the membrane until the permeate became neutral, meanwhile the flux was also monitored. The flow rate of the acidic solution was kept constant at 1 bar. After that, again a liter of 0.1N NaOCL was filtered out of the membrane to clean any bacterial growth. Permeate flux, before and after the regeneration was noted for analyzing regeneration efficiency.

4.3.15 Anti-bacterial:

4.3.15.1 Disk diffusion assay:

The disk diffusion assay is a qualitative method that relies on the diffusion of antimicrobial agents within agar. This is measured by determining the diameter of the inhibition zone, which is

used to ascertain the antimicrobial efficacy of the tested material [37]. If antibacterial substances have positive antibacterial activity, the growth of bacteria will be inhibited and clear visible inhibitory zones will appear as shown in **Figure (15).** The zone of inhibition, which is the location free of bacterial colonization, is situated between the perforated area and the bacterial-cultivated region [38]. Petri dishes and test tubes containing agar were placed in an autoclave at 120°C to prevent contamination during the assay. Once nutrient-uncoagulated agar media was ready, it was transferred to Petri dishes and placed in the refrigerator where it solidified. Afterward, a thin layer of E.coli bacterial was evenly spread on the top surface of the nutrient solid media and then the small parts of coated MMMs were introduced on the media surface and the Petri dishes were placed in a 37 °C warming incubator for a defined duration [39]. The antimicrobial activity of a substance is measured by determining the diameter of the zone of inhibition that is proportional to its efficacy. This method is a simple, reproducible, and reliable testing process. In addition, the cost of supplies and materials is low and economical. In addition, it has good flexibility and can be applied in routine laboratories, making this method the most commonly used. Despite the advantages of the disk diffusion test, a potential disadvantage of using the disk diffusion test as a conventional test method for antimicrobial resistance is that it is relatively slow [40].

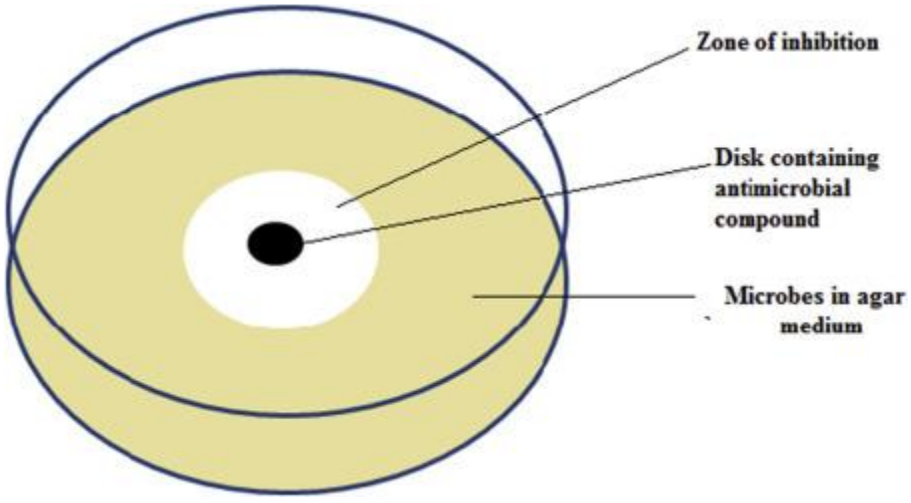


Figure 15. Disk diffusion assay [41]

4.3.15.2. Biofilm inhibition assay :

4.3.15.2a. Qualitative examination:

To examine the qualitative capabilities of MMMs to reduce biofilm formation, the biofilm inhibition assay was conducted. We have used crystal violet dye as primary stain and S. aureus and P. aeruginosa as microbial strains. At first, the MMMs were cut into small pieces and was placed in separate containers along with 24 hours fresh growth suspensions of each microbial strain for three days in incubation at 37.5° C [42]. Afterwards, MMMs were washed twice with 0.2 mL of phosphate-buffered saline (PBS) and dried for 30 minutes. Once dried, 20 ml of a crystal violet (CV 0.1 %) solution was inserted into each MMMs for biofilm formation determination and allowed to stain for one hour. The MMMs were again washed with PBS and ethanol to eliminate excess absorbed CV. Now, with visual inspection of stained MMMs, we can determine the qualitative capacity. The qualitative capacity is directly proportional to amount of stains on the MMMs.

4.3.15.2a. Quantitative examination:

From the continuation of previous experiment, we can determine the quantitative capacity of MMMs to reduce biofilm formation [42]. After washing the stained MMMs. the residual water were stored in a tubes and was centrifuged for 20 minutes at 10000 rpm at 5° C. Then, after separating the precipitate (if any) from the supernatant. Then the bacterial growth in the supernatant was tested by UV-Vis. Then with the difference in the amount of absorbed UV lights or optical density of each MMMs, we can plot a graph (membrane vs OD).

4.3.15.3. Filtration experiment of E.Coli :

A 24 hours fresh culture was prepared by gently shaking 25 mL of Nutrient Broth (NB) and E. coli on a rotary shaker at 20 rpm and 37° C for 24 h. Simultaneously, to attain a concentration of 108 CFU/mL, a saline solution with a concentration of 0.9 % was used to dilute the bacterial solution. Then to examine the ability of the prepared MMMs to reject bacteria, 100 mL of bacterial solution was filtered out in different time intervals in a dead-end setup for 60 minutes at constant 1 bar. Then the collected permeate was spread on NB solid media and was then placed in the incubation at 37° C for 24 h. Then the appeared colonies were counted, and the growth

percentage inhabitation (%) was considered [43]. The removal percentage of bacterial in each membrane was also calculated.

4.3.15.4. Solid surface anti-microbial activity:

To conduct this experiment, first, the ceramic membranes were sterilized using an autoclave. Then the E.coli was spread on the surface of the MMMs and the membranes were rested on a petri dish and then kept in an incubator at 37° C for 24 hours [44]. After that, the bacteria-coated MMMs were shaken in 0.9 % NaCl solution for an hour at 150 rpm. Afterward, the membranes were removed from the solution and the solution was diluted in two concentrations (10X dilution and 100X dilution). The dilutions were spread onto the surface of 24 h fresh solid media and then incubated for 24 h at 37° C then the CFU was counted.

Chapter 5

5. RESULTS AND DISCUSSION

In this chapter, we have stated the findings of our study based on the information we gathered from the results of the methodologies we applied. We have also analyzed and interpreted the meaning of the data collected and put them in context. We have also explained the benefits of the findings.

5.1 Characterization of nano-particles:

5.1.1. Adsorption isotherm: From the N2 adsorption isotherm **(Fig. 16a),** it can be concluded that the NPs are porous, having type-IV isotherm with H2-type hysteresis loop. This denotes that the material is mesoporous.[35]

5.1.2. BET Analysis: NPs had a BET surface area of 93 m2/g and half pore width of 1.96 nm. However, NLDFT pore size distribution suggests occurrence of some micropores **(Fig. 16b).** [35]

5.1.3. XPS Analysis: Long scan of XPS shows **(Fig. 16c)** peaks of Mg 2p, Mg 2s, Al 3p3/2, Al 2s, Ti 3p, Ti 2p3/2, Ti 2p1/2.[35]

5.1.4. XRD Analysis: In the XRD patterns **(Fig. 16d)**, distinct peaks are visible which correspond to cubic phase of MgO (002) and (202) planes of cubic MgO are evident from peaks at 43° and 62°[35].

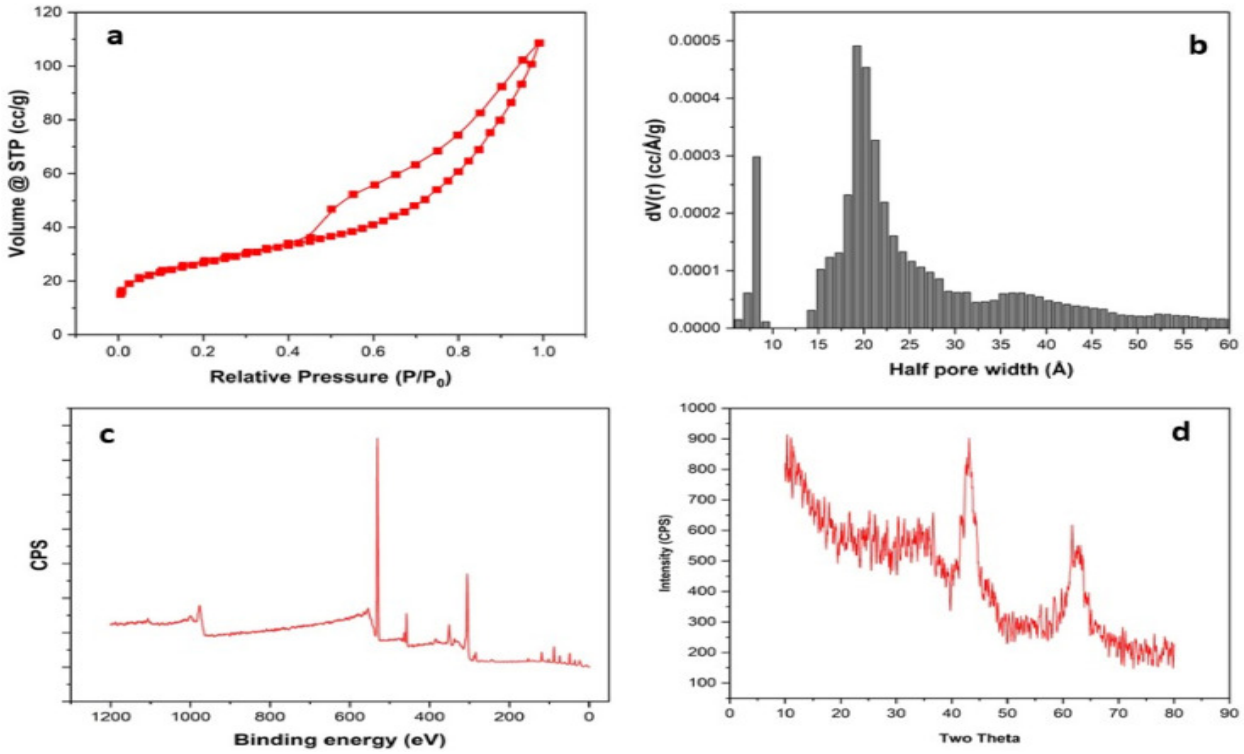


Figure 16. a) Adsorption Isotherm of NP, b) BET Analysis of NP, c) XPS Analysis of NP, d) XRD Analysis of NP.

5.1.5. TEM Analysis:

UHR-FEG-TEM (ultra-high resolution field emission gun transmission electron microscope) was used to investigate the morphology of the NPs. TEM images and EDX spectrum have been provided in **Figure (17).** The presence of Mg, Al, Ti and O is visible from the TEM-EDX spectra confirm the presence of Mg, Al, and Ti in the sample. TEM images showed honeycomb-like pores and some wormhole-like morphology. Higher magnification shows particle size ranging from 9 to 10 nm. pH of zero-point charge (pHzpc) was determined to be ~13. High pHzpc allows adsorbents to have net positive surface charge at higher pH points (<13). This property becomes useful in capturing anions with high pKa values and throughout a broad pH range. [35]

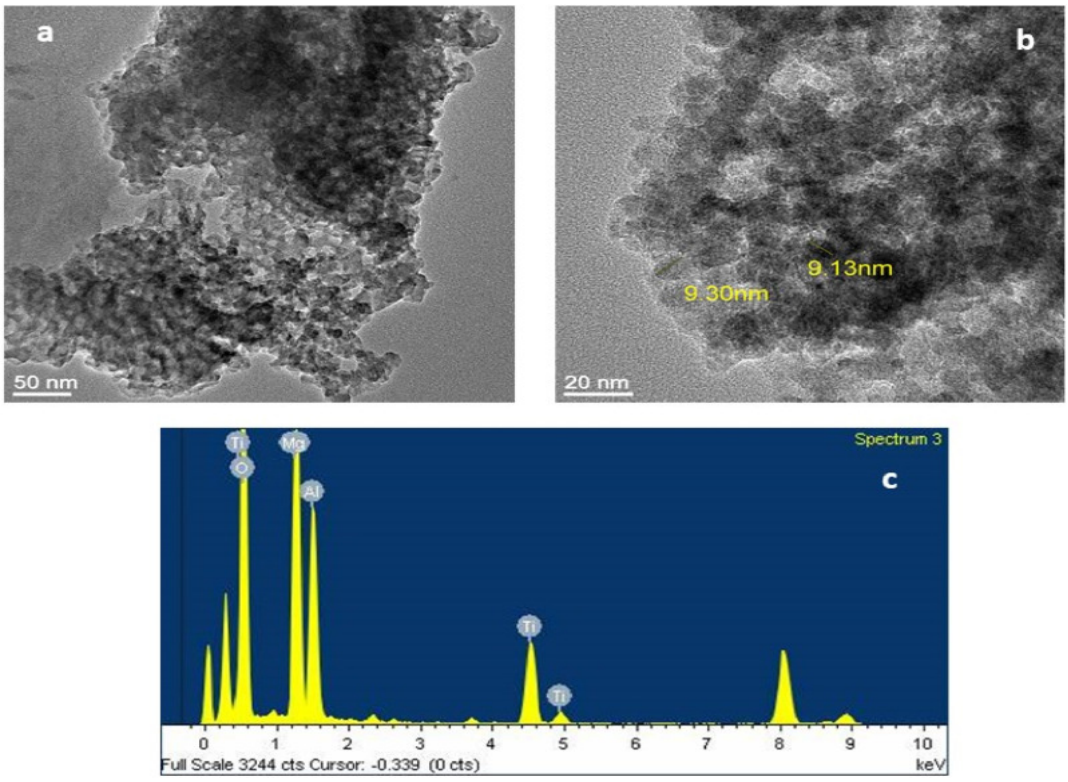


Figure17. Images of TEM and EDX spectrum of NPs.

5.1.6. Heavy metal ion competition:

The actual contaminated drinking water is more complex in composition, there are many other heavy metal ions present in the water. The coexisting ions are also an important factor affecting the removal capacity of nanoparticles. To examine the removal percentage of multiple heavy metal ions, we have divided the experiments into three categories, namely total multi-metal, binary multi-metal, and ternary multi-metal. The experiments were performed in batch adsorption setup at room temperature to capture the removal percentage performance of mesoporous Mg–Al–Ti composite oxide nanoparticles. From **Figure (18)** it can be stated that in binary ionic competition, in a set of both anions almost 100 % As was removed in all the concentrations, whereas, the removal percentage of Cr was notably decreasing while increasing the concentration (1 ppm-82 %, 10 ppm-71 %, 20 ppm-55 %). In the set of anions and cations, the cations were removed with almost 100 % results in all concentrations, whereas the As ions removal percentage fluctuated. In the set of both cations, the removal percentage of both the metal ions was almost the same in all concentrations. Now, examining the data from the **Figure (19)** ternary multi-metal batch adsorption capacity test. From the first set which has one anion and two cations, we can see that both cations (Cd, Pb) are 100 % removed, whereas the anion (Cr) removal percentage is decreasing with the increase in the concentration (1 ppm-73 %, 10 ppm-60 %, 20 ppm-36 %). Looking at the second set, there is a set of one anion (As) and two cations (Cd, Pb). In this setup the results are as before, the only notable difference is that the anion (As) removal percentage is more than Cr. Advancing to the last set of ternary multi-metal ion competition where there are two anions (As, Cr) and one cation (Pb). From its results, we can conclude that As ion and Pb ions were almost 100 % removed in all concentrations, whereas the Cr removal percentage was declining with an increase in the concentration. With the information gathered from the sets of binary and ternary data, we can conclude that the mesoporous Mg–Al–Ti composite oxide NPs adsorbs more cations than anion but the only anion that performed better in all sets is As(iii). Now, coming back to examine the last data set of multi-metal ion competition is total multi-metal ions. Concluding from the data available in **Figure (20)**. We can state that in the presence of all anions and cations, all the ions were removed close to 100 % but only Cr was less adsorbed reflecting less removal % with an increase in concentration (1 ppm-95 %, 10 ppm-88 %, 20 ppm-71 %). Hence, we can claim that mesoporous Mg–Al–Ti composite

oxide NPs are capable of removing multi-metal ions and can filter the contaminated drinking water.

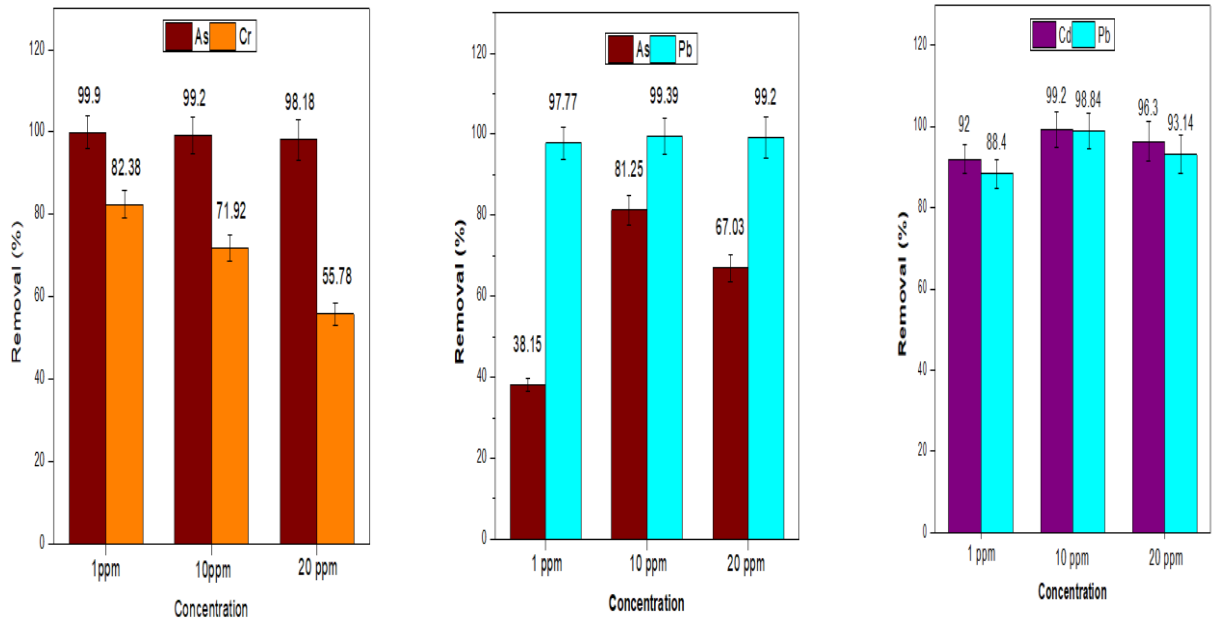


Figure 18. Removal percentage of Binary Multi Metal

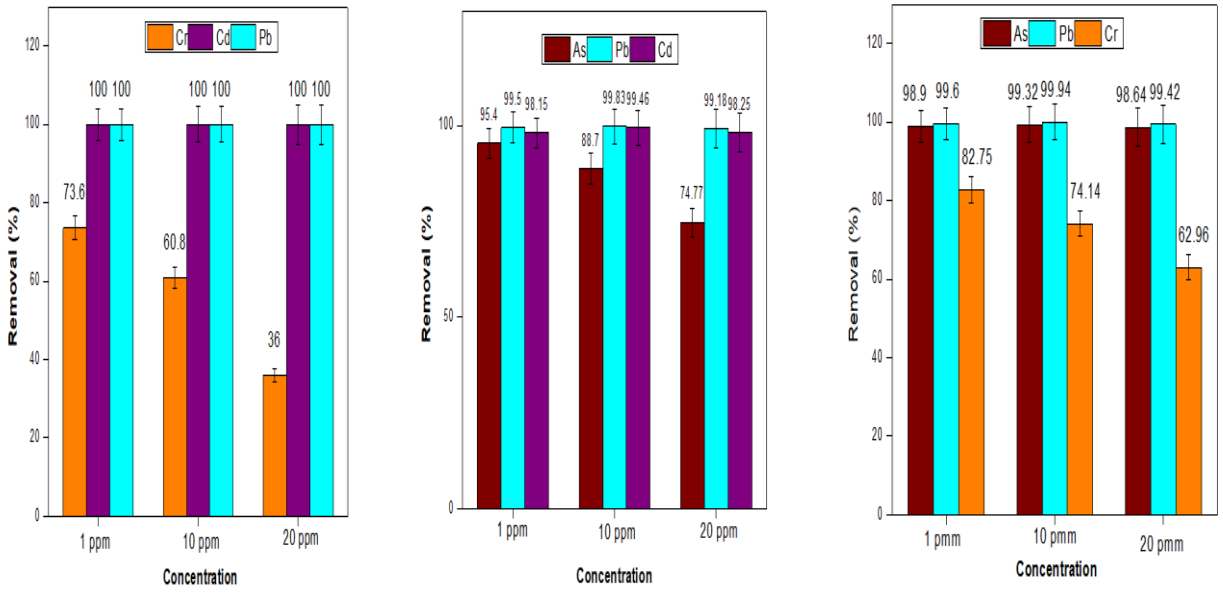


Figure 19. Removal percentage of Ternary Multi Metal

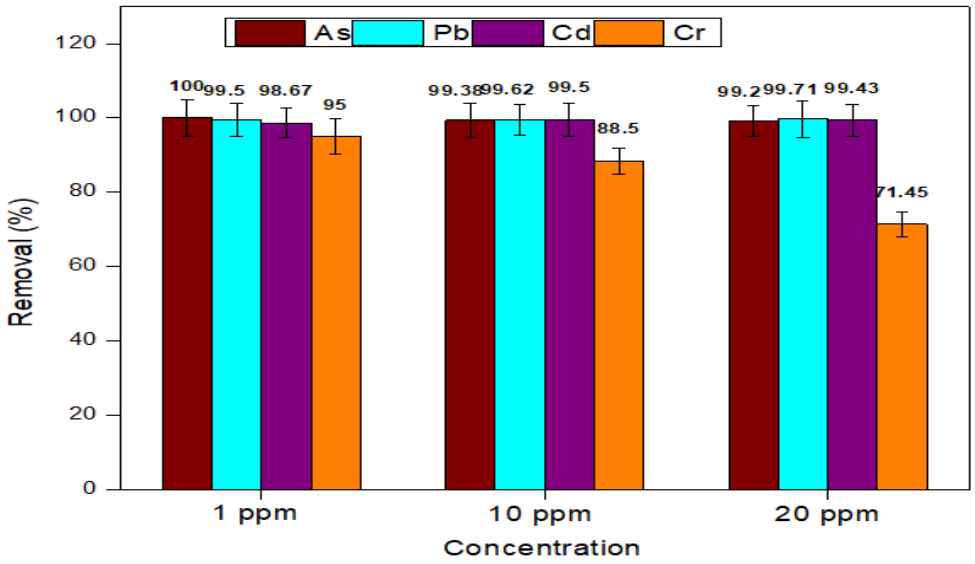


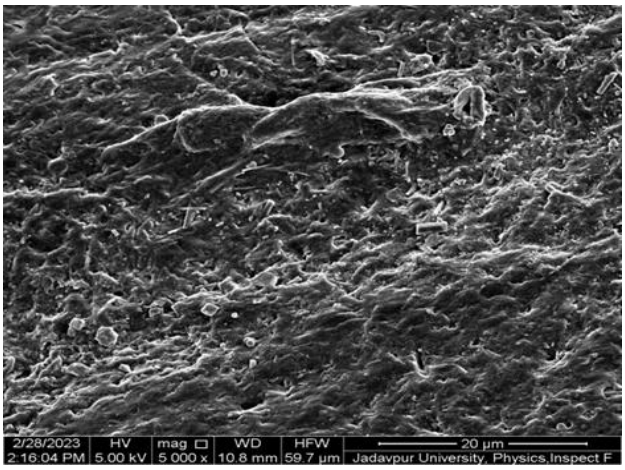
Figure 20. Removal percentage of Total Multi Metal

5.2 Characterization of MMMs

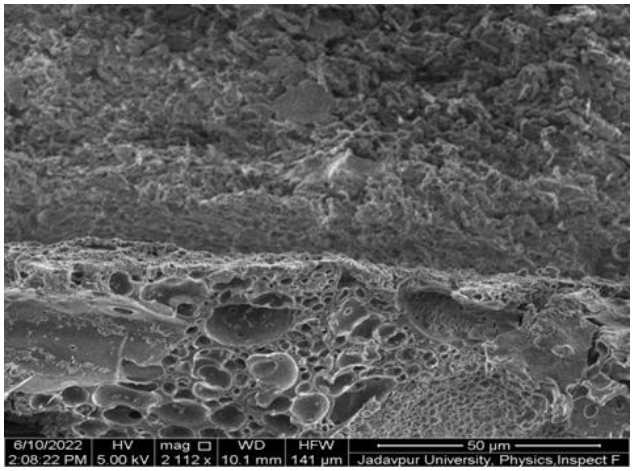
5.2.1. FESEM Analysis:

FESEM images and FESEM-EDX mapping have been used to probe into the membrane morphology and incorporation of the NPs. The FESEM images of the top surface, and cross-sections before and after adsorption of heavy metal of the three prepared MMMs are shown in **Fig (21).** From the FESEM images we discovered the polysulfone blend membrane coating has a smooth yet porous surface which means the coating has not blocked the pores and was homogenous. Hence, NPs were homogeneously distributed in the polysulfone blend membrane. The cross-sectional view of PSF suggests that the membrane has a more spongy structure which leads to more permeate flux. The in-situ membrane's surface FESEM images shows cluster or flat pebbles-like structure with relatively larger, non-uniform pores. The FESEM image of the PVA membrane discovered that the NPs were not visible and the surface was less porous and smooth, its cross-sectional view shows that the nanoparticles are equally distributed in the membrane leading to almost uniform size of pores and smooth, uniform layer of coating on the surface. EDX mapping **(Fig. 22)** shows the uniform distribution of incorporated nano-particles in

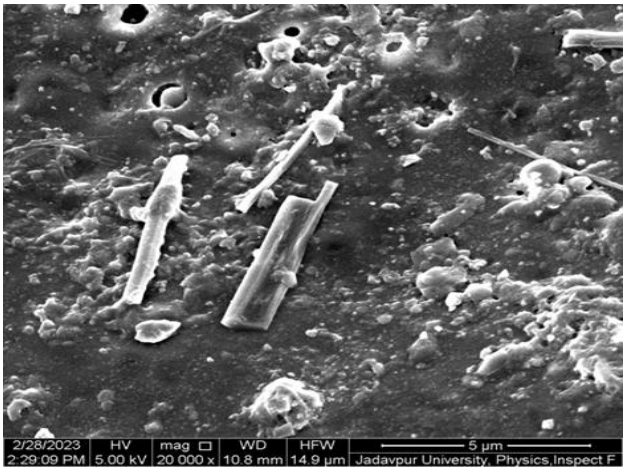
all three MMMs. The concentration of NPs is higher in the inner and outer surface of PVA and polysulfone blend membrane which may result in low NPs leaching and hence, better separation performance. The concentration of NPs was in the middle of the In-situ membrane, this may result in increased porosity of the membrane. The FESEM and EDX mapping images after As adsorption **(Fig. 23)** show the presence of As in the MMMs and the overall structure of the MMMs was in good condition.



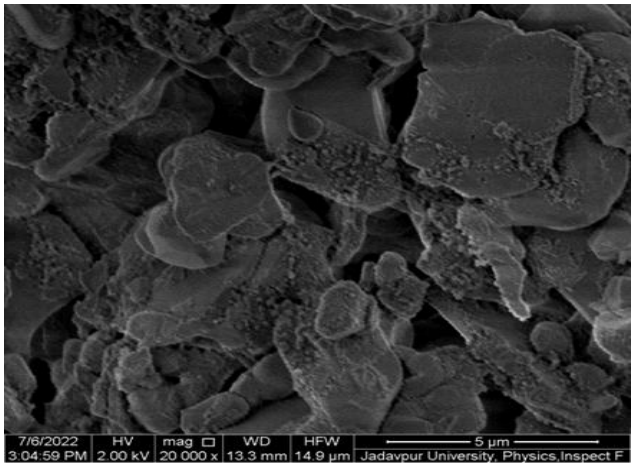
PSF Surface



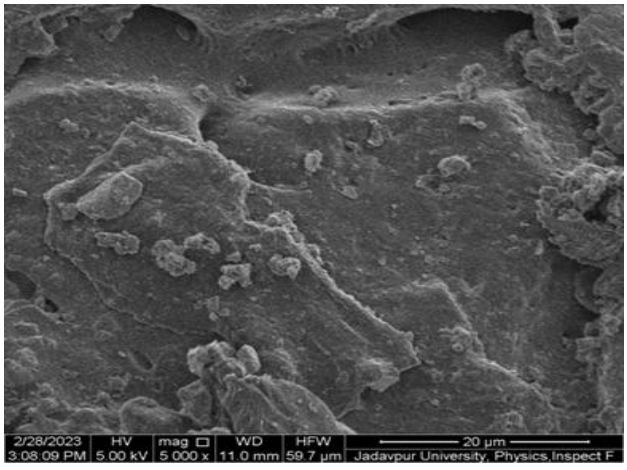
PSF Cross section



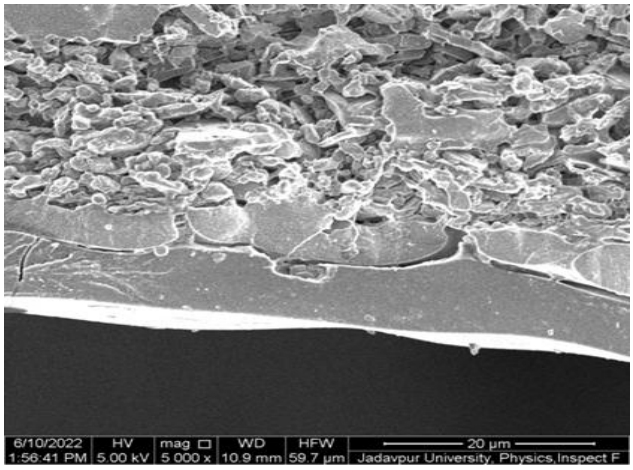
PSF after As adsorption



In-situ surface



PVA Surface



PVA Cross section

Figure 21. Surface and cross-sectional FESEM images of all three MMMs.

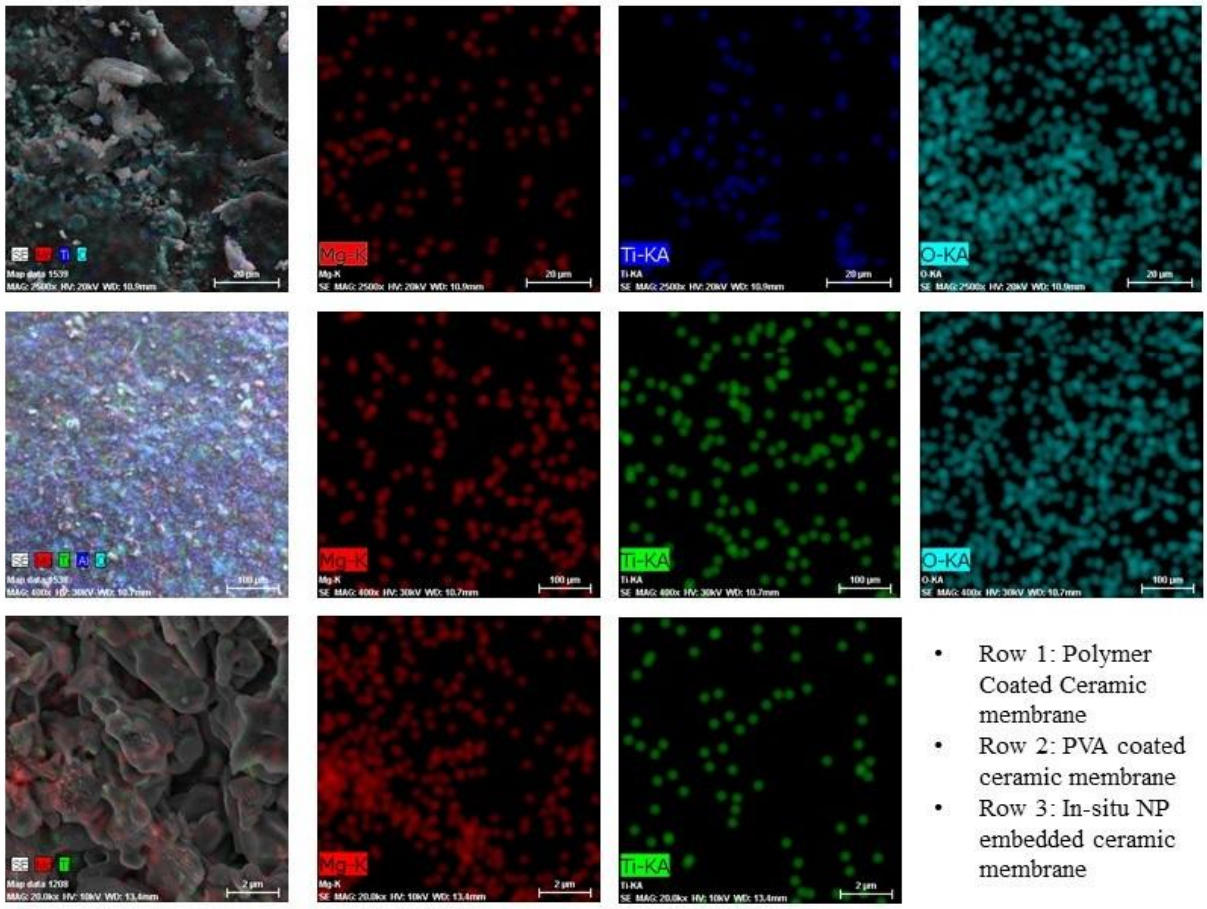


Figure 22. FESEM & EDX mapping images of all three MMMs surface.

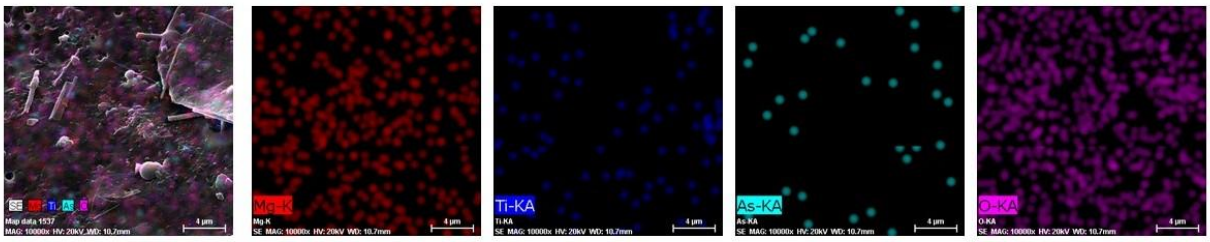


Figure 23. FESEM & EDX Mapping after As adsorption

5.2.2. XRD Analysis:

The crystal structures of the prepared MMMs were examined by X-ray diffraction technique (XRD) **Figure (24).** The four obvious diffraction peak locations indicate that both the membranes are crystalline in structure but the peak intensity of TiO_2 is lower than Al_2O_3 and MgO is consistent with the results. This denotes that the periodicity of atoms in TiO_2 is also lower than Al_2O_3 and MgO. However, corresponding to the main diffractions of TiO_2, the crystallinity structure can also be identified. Hence, the TiO_2 has an anatase phase peak at (101) at an angle of 25° [45]. Since, the XRD peak for alumina (Al_2O_3) varies depending on its phase, with the most common phase being α-alumina and γ-alumina. For α-alumina, the XRD- pattern typically shows peaks corresponding to the (012), (104), (110), (110), (113), and (024) planes, which are indicative of hexagonal crystal structure [46]. As we have (104) plane for Al_2O_3, it can be stated that our Al_2O_3 NP is in α-alumina having a hexagonal crystal structure. The peak locations of MgO were representing (200) and (220) sets of lattice planes [47]. The absence of any other peak substantiated the purity and invariable incorporation of the calcined NPs.

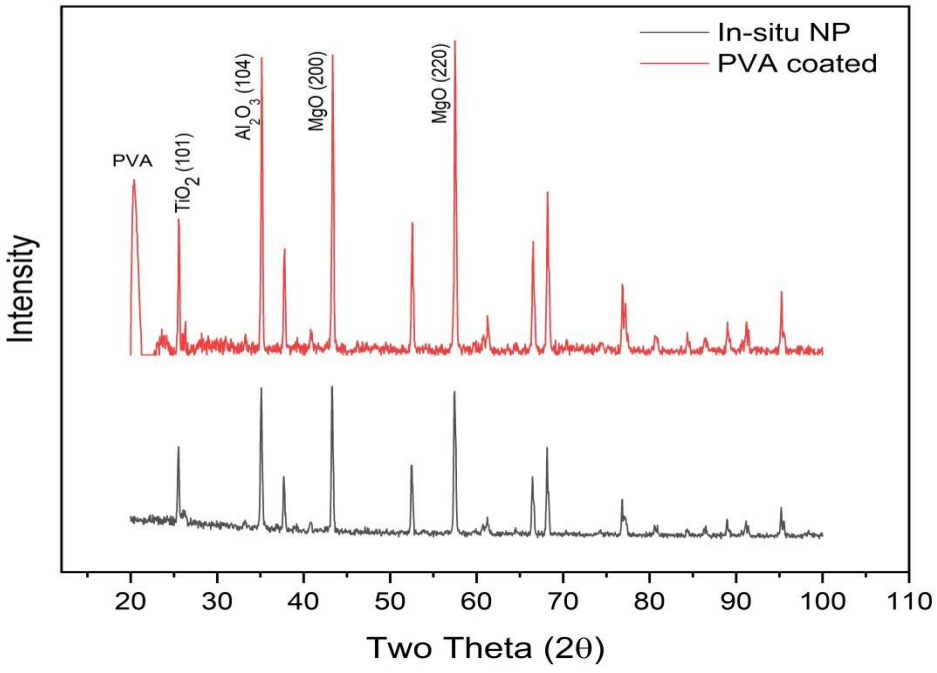


Figure 24. XRD image of MMMs.

5.2.3. Contact Angle

As shown in **Figure (25)** the contact angle of the membranes is 62.13° for non-modified membrane, 25.06° for in-situ membrane, 69.83° for PSF blend membrane, and 38.58° for PVA membrane. Analyzing the CAs of all three membranes, it can be concluded that all three MMMs are hydrophilic. Hence, all three MMMs are ideal for water filtration. It can also be seen that in situ and PVA membranes are more hydrophilic than the non-modified membrane. This proves better incorporation of NPs and increased surface roughness in these two membranes. As we can see the non-modified ad PSF blend membrane has properly spherical shaped water droplets compared to Insitu and PVA membrane. With this information, we can say that insitu and PVA membrane has less surface tension compared to other membranes.

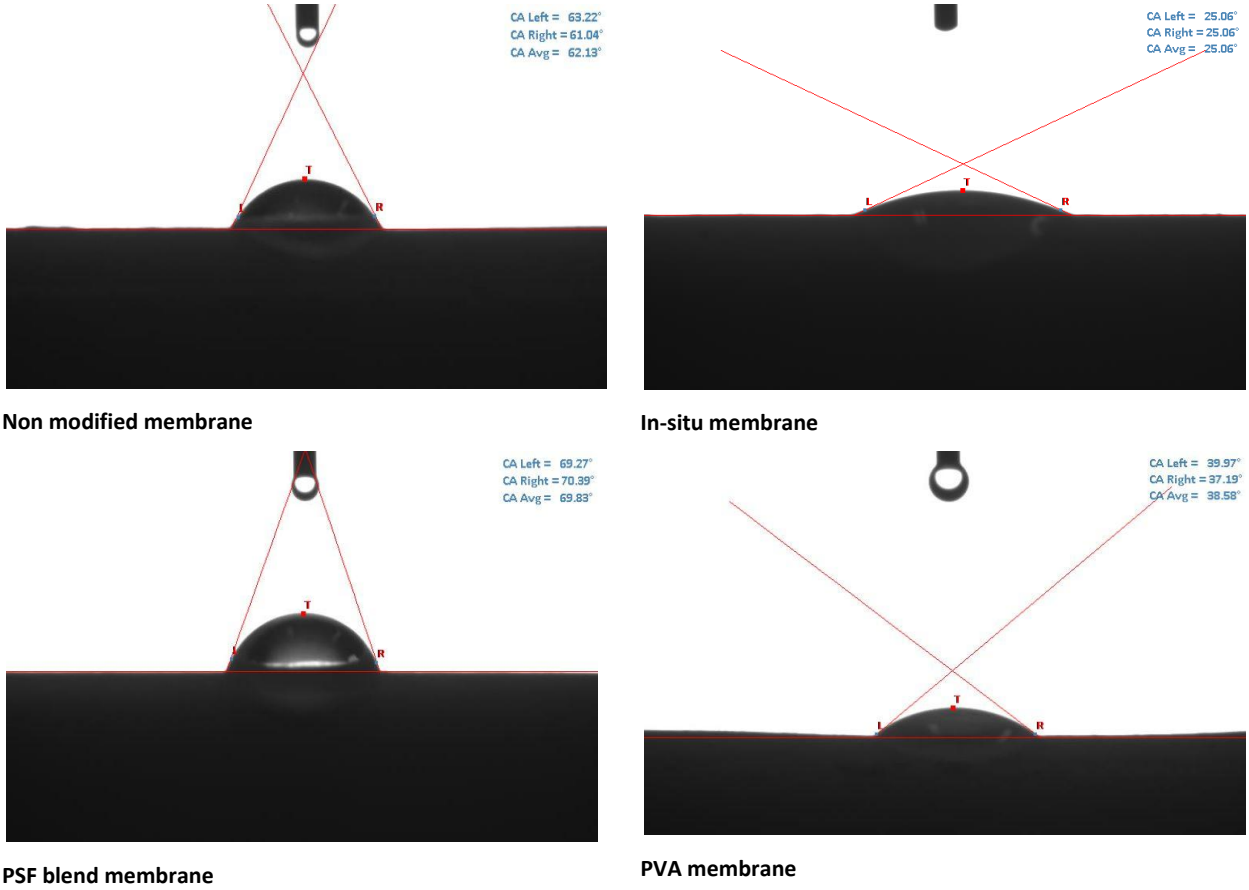


Figure 25. Contact angle of unmodified and all three MMMs

5.2.4. Pure water flux:

Pure water flux was investigated in all three MMMs as a function of pressure and water flux **(Figure 26)** [48]. PWF was calculated at different intervals until the flux reached equilibrium at different range pressures. At 100 bar all three MMMs reached their equilibrium in around 40 minutes. With the graph, we can conclude that the flux is increasing with increasing pressure in all three MMMs. This shows the dispersion of NPS in the MMMs. Precisely we can depict that the NPs are scattered on the surface without agglomeration and pore blocking of membranes. Comparing the flux of membranes with each other, we can see that the in-situ membrane has a visibly higher flux than the polysulphone blend membrane followed by the PVA membrane. This can be explained by the hydrophilicity of the membranes.

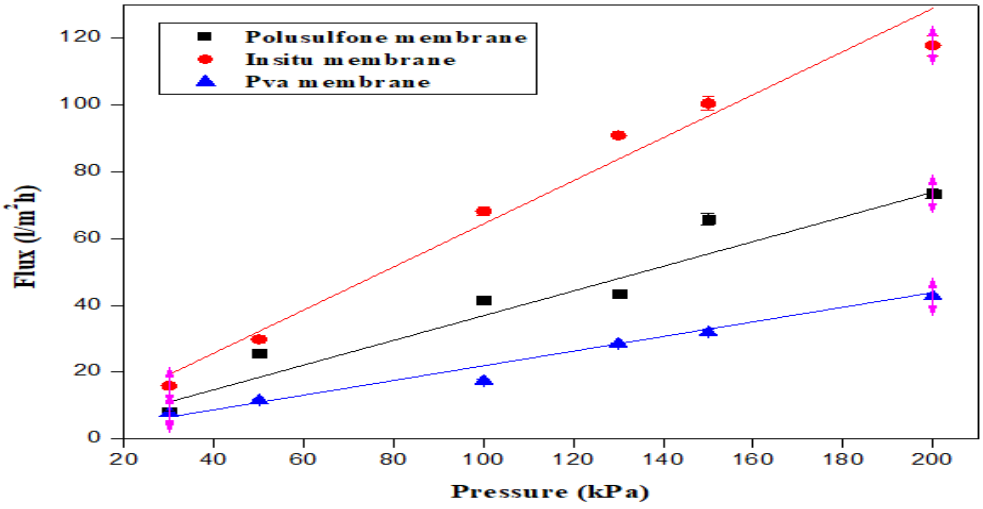


Figure 26. Flux Recovery of All Three MMMs at Different Pressure.

5.2.5. pH Experiment:

This experiment was conducted to check the As rejection capacity of the MMMs in different pH. **Fig.27** shows the graphical representation of As concentration and removal percentage in different pH. From the data collected, it can be stated that all three MMMs show almost 100 % removal percentage. It is to be noted that all three MMMs showed the same As rejection in all pH ranges. Hence, it can be claimed that all three MMMs have good As rejection capacity in all pH ranges.

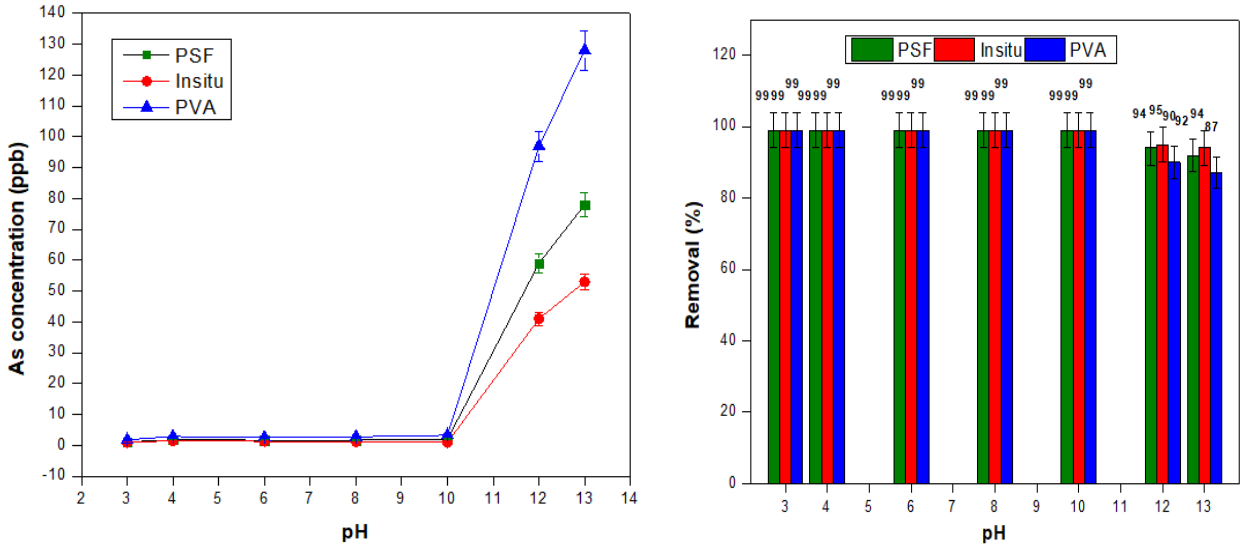


Figure 27. As concentration in pH (left), As removal percentage in different pH (right).

5.2.6. Anti-fouling:

The anti-fouling property of prepared MMMs was examined at room temperature in a dead-end setup with 1000 ppm BSA solution. Due to the fouling tendency of the prepared MMMs, there is a difference between pure water and BSA solution fluxes**.** After BSA solution permeation, the MMMs were washed with warm DI water then again pure water flux was restored at different levels. From the data collected from the experiments in **Figure (28a)**, it can be stated that the in-situ membrane has better flux compared to the other two membranes. This is due to its better hydrophilicity and good anti-fouling properties of the membrane, as the flux before and after the BSA solution is almost the same. 35.35 l/m^2h is the DI water flux of the in-situ membrane before the BSA solution and 30.79 l/m^{2}h is the DI water flux after the BSA solution of the membrane. As shown in **Figure (28b)** it can be seen that in FRR PVA membrane is leading with 89.87 %, followed by the in-situ membrane with 87.09 %, and at last PSF blend membrane with 79.16 %. The values of reversible, irreversible, and total fouling are also mentioned in **Figure (28b)** and **Table no. (03).** Polysulfone blend membrane has the highest percentage of reversible fouling with 79.16 %, irreversible fouling with 12.26 % and total fouling with 33.09 %. Hence, values of R_{ir}, R_r, and R_t are the highest in the PSF blend membrane followed by in-situ and at last PVA membrane.

Table no.3. Fouling resistance ratios of the MMMs.

Membrane	J1(l/m^{2}h)	Jp(l/m^{2}h)	J2(l/m^{2}h)	FRR(%)	R_{ir}(%)	R_r(%)	R_t(%)
PSF Blend	20.09569	13.4443	15.90909	79.16	20.83	12.26	33.09
In-situ	35.354	26.5151	30.79179	87.09	12.90	12.09	25
PVA	8.59950	7.667032	7.729113	89.87	10.12	0.72	10.84

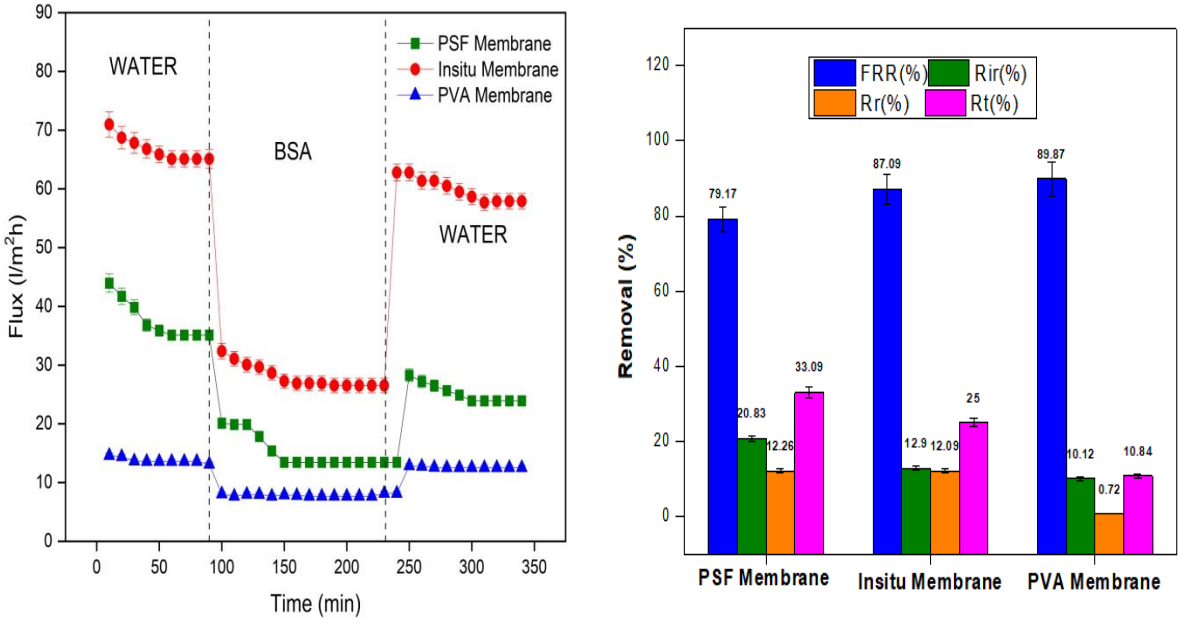


Figure 28. a) Water flux recovery of the MMMs before and after BSA permeation (Left) b) fouling resistance ratios of the MMMs.

5.2.7. Long term filtration: We have done a long-term experiment test of the in-situ membrane to know the breakthrough volume of the membrane. From **Fig. 29**, we can say that the membrane got exhausted after filtering 4.5 liters of 100 ppb As solution at constant pressure (1 bar) during continuous operation. It is also to be noted that with the number of each As solution filtration cycle, the flux is declining as shown in **Fig.29**. With this information we can state that the membrane is gradually getting exhausted with the increasing number of filtration cycles. However after regeneration, the membrane filtered out about 2.5 L of 100 ppb As solution.

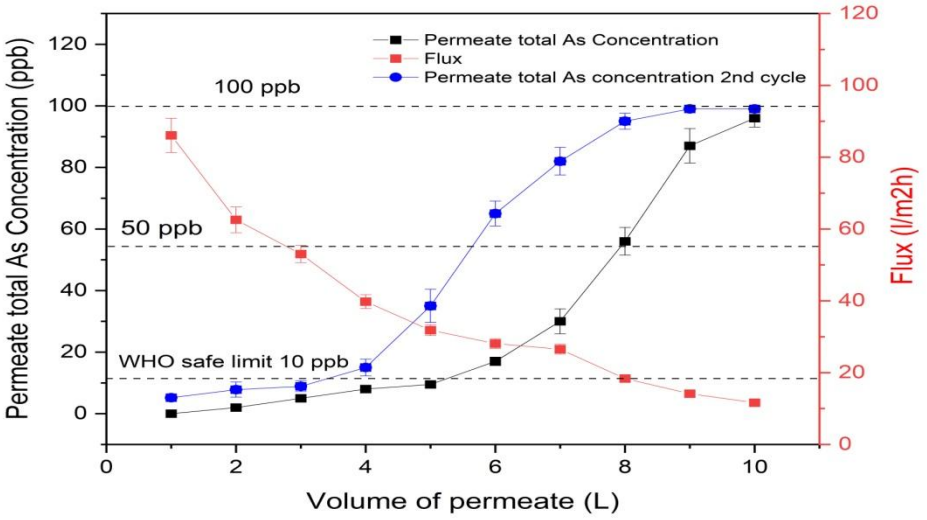


Figure 29. Long term filtration of in-situ membrane

5.2.8. Regeneration:

After a long-term filtration experiment, the membrane was regenerated. The regeneration was done with the acidic solutions while monitoring the flux. From **Fig.30** it is evident that the flux of 0.1 N NaOH solution is predominantly increasing with time at constant pressure (1 bar). The solution 0.1 N HCL was to neutralize the pH of permeate, to ensure that the NaOH is washed out of the membrane.

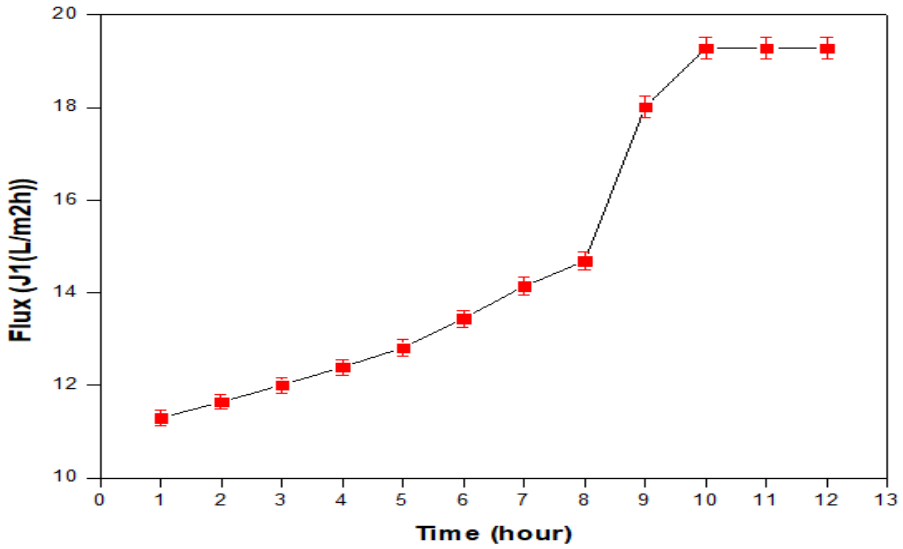


Figure 30. Regeneration of In-situ membrane in NaOH solution.

5.2.9. Anti-Bacterial:

5.2.9.1. Disk diffusion assay:

In **Figure 31** the inhibition zone of all MMMs and control membrane is visible. Since all MMMs have shown the diameter of the inhibition zone, hence we can conclude that all MMMs have positive antibacterial activity. However, in the PVA membrane, more clear inhibitory zones have appeared. After PVA, the PSF blend membrane's inhibitory zone is clearly visible, however, the in-situ membrane inhibitory zone is not clear enough as compared to the other two membranes. This may be due to the NPs incorporated coating layer of the PVA and PSF membrane, as this assay tests the antimicrobial property of the surface of the MMMs and the in-situ membrane doesn't have a proper NPs incorporated layer on it.



Figure 31. Disk diffusion assay of all MMMs.

5.2.9.2. Biofilm inhibition assay :

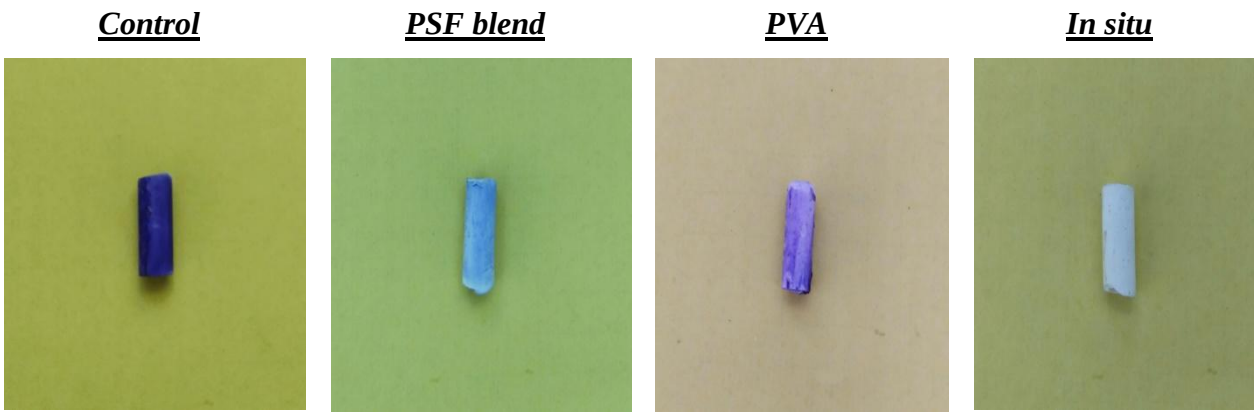


Figure 32. Qualitative examination

From **Figure (32)** we can examine the qualitative measurement of the MMMs, it is clearly visible that the unmodified membrane has exhibited more CV stains as compared to other modified membranes. Now, among all three modified membranes in-situ membrane is the clearest among all membranes, followed by PVA, PSF blend membrane. This is an indication that in-situ membranes have less biofilm formation on the surface. Hence, it can be stated that all three MMMs have good anti-bacterial properties of biofilm formation. In quantitative examination **(Fig.33)** results also, the in-situ membrane shows less UV light absorption, which once again assures that among all three MMMs, in-situ has the best anti-bio-film formation property. However comparing the qualitative and quantitative results of PSF and PVA membranes, the results are not matching. As in qualitative, CV stains are more visible in PVA than PSF but the quantitative results show that PSF has absorbed more UV light than PVA which means PSF had more bacterial inhibition. This may due to the hydrophilic property of PVA membrane (assured by contact angle results) that the stains are stuck in the pores of the surface which makes it more visible at some spots. However the PSF blend membrane has a smooth surface, when the membrane was washed after the staining, most of the bio-film formation was washed off and was collected as residual water for UV-Vis inspection. Hence, the PSF quantitative results show more UV-light absorbance. Now with this information, it can be stated

that though PSF membrane have more qualitative results, the membrane can be easily restored by washing it with 70% ethanol.

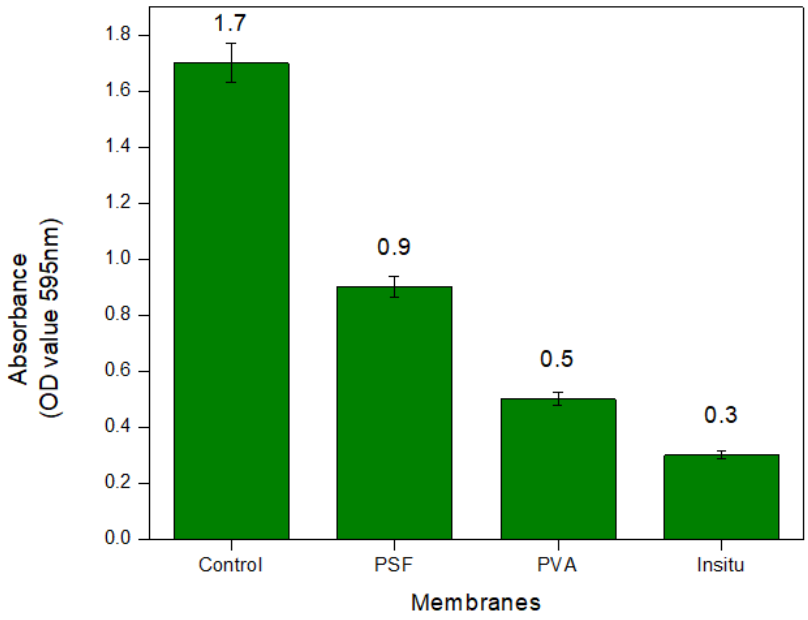


Figure 33. Quantitative examination

5.2.9.3. E.coli filtration examination

Table 4. CFU Count of MMMs after filtration.

Time (min.)	PSF (CFU/ml)	PVA (CFU/ml)	Insitu (CFU/ml)
10	53	11	04
20	42	09	01
30	35	07	00
40	17	05	00
50	10	03	00
60	07	02	00

Table 5. Bacterial Removal percentage of MMMs.

Time (min.)	PSF Removal (%)	PVA Removal (%)	In-situ Removal (%)
10	50.92	89.81	96.29
20	61.11	91.66	99.07
30	67.59	93.51	100
40	84.25	95.37	100
50	90.74	97.22	100
60	93.51	98.14	100

CFU count and removal percentage of E.coli solution's permeate with time are shown in **Fig.34** and **Table no.4&5**. Accordingly, it can be noted that as the time is increasing, the CFU is decreasing. With these results, we can conclude that the membranes are rejecting bacteria and this result is supported by the removal percentage graph **(Fig. 34)** as the graph shows the removal percentage is increasing with time. However, when the removal percentage of all MMMs is compared, the in-situ membrane has the highest anti-bacterial properties followed by the PVA membrane and then the PSF blend membrane. Moreover, the pictorial representation of the microbial cell viability inhibition in the time-variant of all three MMMs is shown in **Figure 35**.

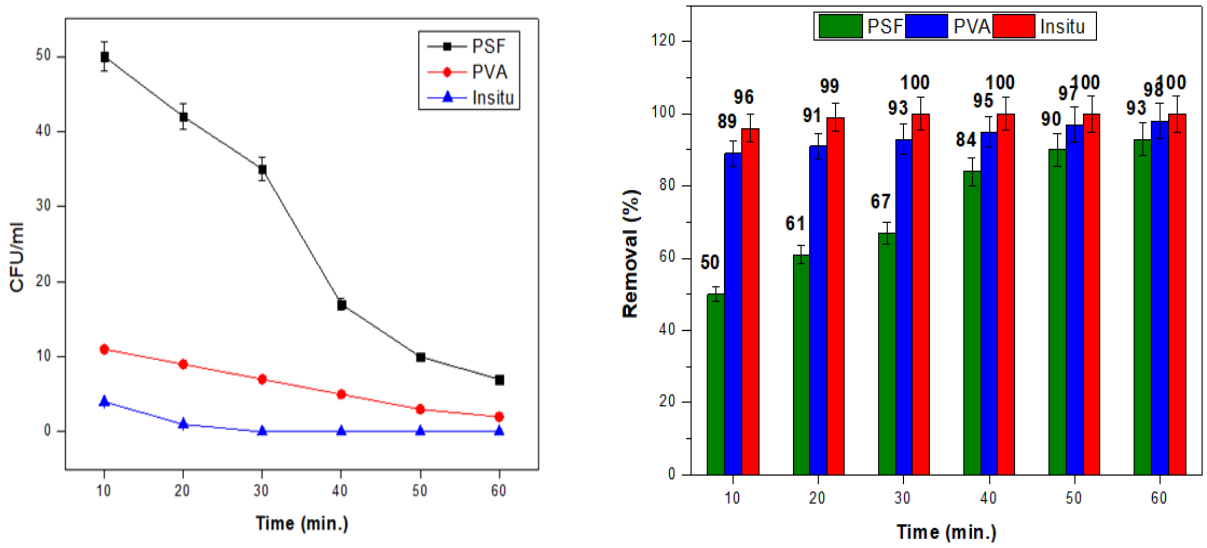
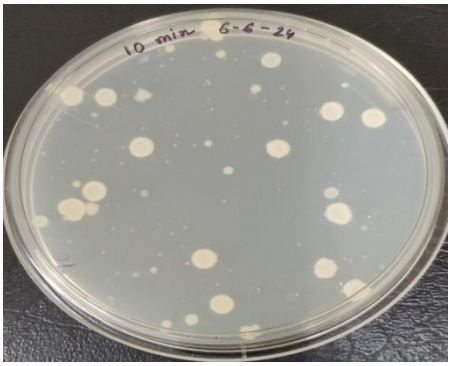
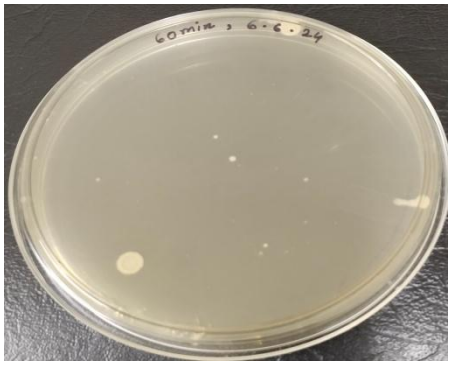


Figure 34. CFU Count of MMMs after filtration (left), bacterial Removal percentage of MMMs (Right).

PSF 10 min.

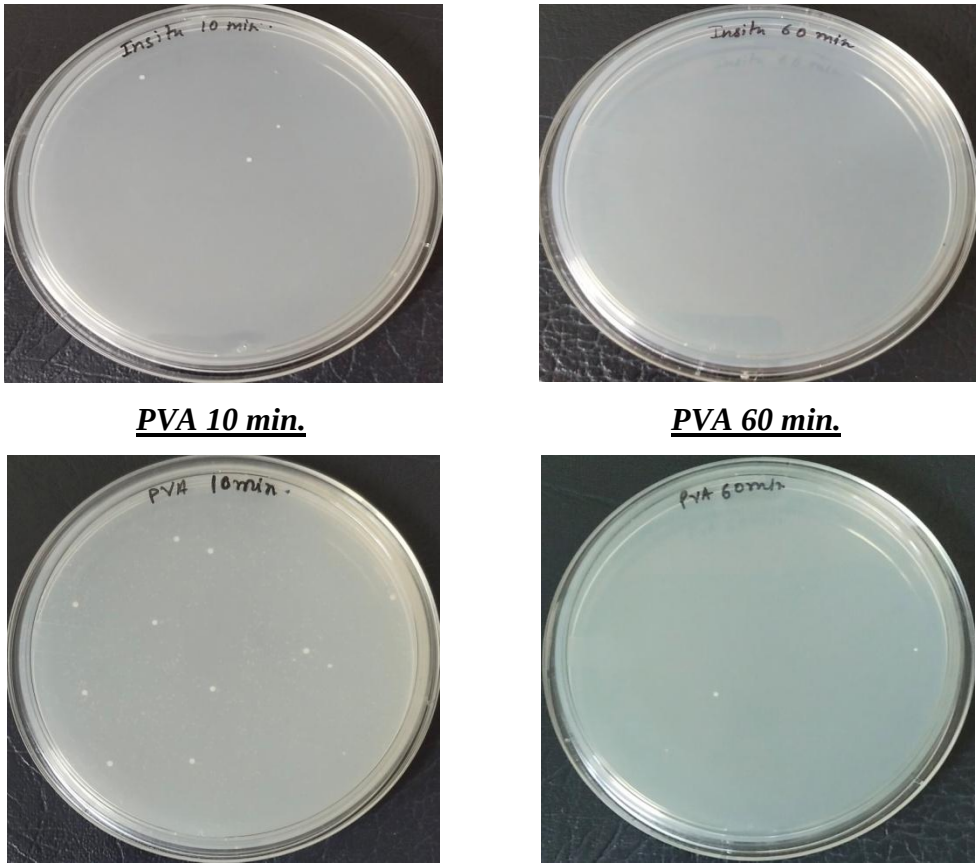


PSF 60 min.



In-situ 10 min.

In-situ 60 min.



PVA 10 min. ***PVA 60 min.***

Figure 35. Microbial cell viability inhibition in time variant of all three MMMs.

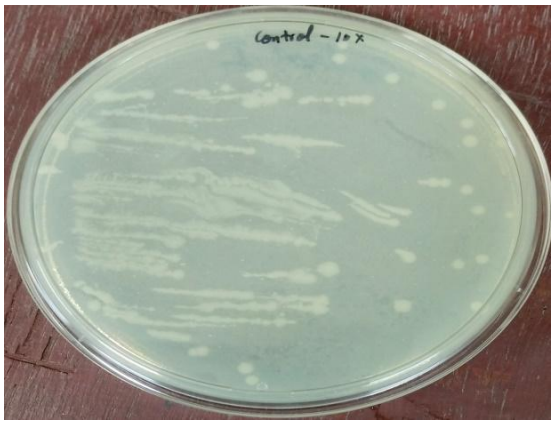
5.2.9.4. Solid surface antimicrobial activity:

This experiment was conducted to measure the antimicrobial activity property of membrane's surface by counting the CFUs of NaCl solution washed off residual water of bacteria-coated membranes. As data from **Table No. 6** and **Figure 36** shows in-situ and PVA membranes have good surface antimicrobial activity. However, the polysulfone membrane has uncountable CFUs which can be due to two reasons, either the PSF membrane was incapable of killing E.coli or the NaCl solution thoroughly washed off the bacteria from its surface. If we consider previous experiments then according to contact angle and disk diffusion assay data, there is a high chance that the results are due to its surface smoothness. Briefly, it can be stated due to the PSF membrane's smooth surface the bacteria was unable to enter inside the membrane and remain on

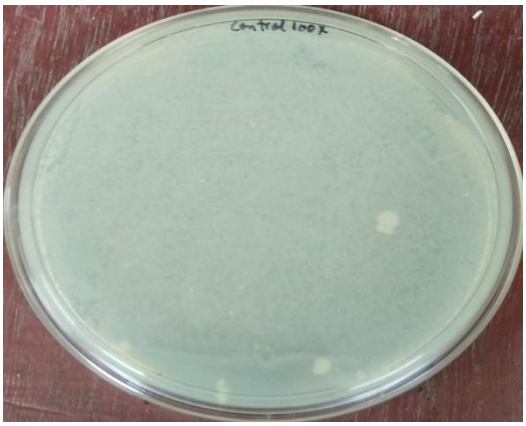
the surface due to which it did not interact with enough NPs. Hence, when NaCl solution was used to wash the membrane, all the bacteria were washed off in the NaCl solution and resulted in uncountable CFUs in both 10 and 100 times dilutions.

Table no.6. CFU count of membranes in 10&100 times dilutions.

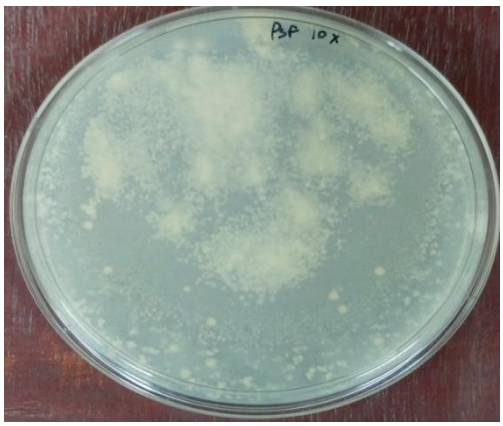
Membranes	**CFU in 10 times dilution**	**CFU in 100 times dilution**
Control	Uncountable	7
PVA	14	2
Psf blend membrane	Uncountable	Uncountable
Insitu	0	0



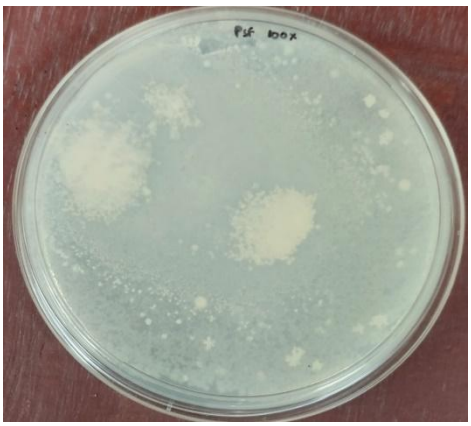
Control 10X



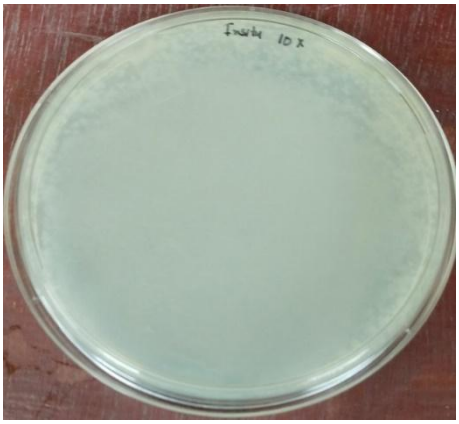
Control 100X



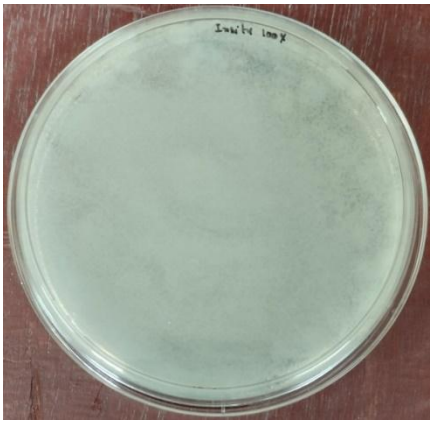
PVA 10X



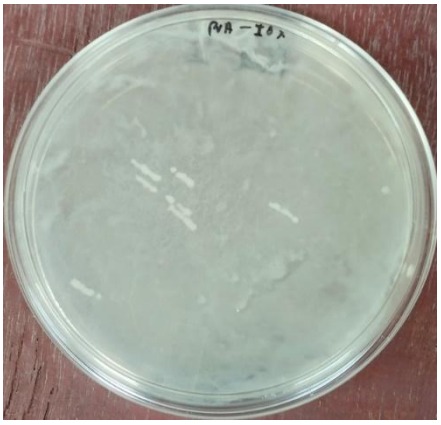
PVA 100X



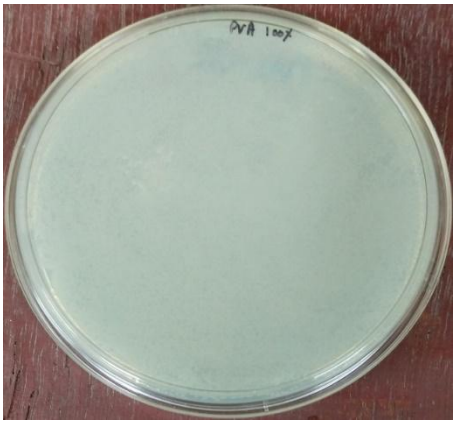
In-situ 10X



In-situ 100X



PVA 10X



PVA 100X

Figure 36. Antimicrobial activity of all membrane's surface .

CHAPTER 6

Conclusion

Mesoporous Mg–Al–Ti composite oxide NPs were synthesized using a self-assembly synthesis with a soft template. NPs showed excellent multi-metal ions (As, Pb, Cd, Cr) removal capacity for both cationic and anionic in batch adsorptions. The NPs were successfully incorporated into the polysulfone blend membrane, in-situ-formed membrane, and PVA membrane using a simple sol-gel method. The characterization of NPs was already discussed in reference no. 35, the NPs adsorption capacity was tested for multi-metal (As, Pb, Cr, Cd) ions in binary, ternary, and total heavy metal batch setup, which showed excellent results in all concentrations. Again, the Arsenic adsorption properties of NPs incorporated MMMs were thoroughly studied in the effect of pH, where all the membranes showed 99% removal percentage in all ranges of pHs. Membranes having a contact angle of 25.06º for insitu, 69.83º for PSF, and 35.58º for PVA are evident to state the hydrophilic property of the membranes. 79% of Psf, 87% for In-situ, and 89.87% for PVA membrane flux recovery ratio after BSA solution filtration shows good anti-fouling properties of all MMMs. Long-term filtration showed a breakthrough volume of 4.5 L while filtering 100ppb As solution and the flux was declining with the addition of no. of filtration cycles. The regeneration was done successfully by increasing the flux of the membrane with the help of acidic solutions and the long-term filtration of the regenerated membrane showed breakthrough volume of 2.5 L. The anti-bacterial property was tested by doing experiments like disk diffusion assay, biofilm formation assay, E.coli filtration, and solid surface antimicrobial property. In the anti-bacterial property test in-situ membrane showed better results than the other two membranes, altogether all three MMMs showed good anti-bacterial properties. To conclude, it can be claimed that with these multifunctional properties and capacity to remove multiple heavy metal ions along with arsenic and bacteria, the MMMs are excellent alternatives for an economically friendly water treatment process.

CHAPTER 7

References

1. Alka, S., Shahir, S., Ibrahim, N., Ndejiko, M. J., Vo, D. V. N., & Abd Manan, F. (2021). Arsenic removal technologies and future trends: A mini review. *Journal of cleaner production*, *278*, 123805.
2. Qasem, N. A., Mohammed, R. H., & Lawal, D. U. (2021). Removal of heavy metal ions from wastewater: A comprehensive and critical review. *Npj Clean Water*, *4*(1), 1-15.
3. Sharma, S., & Bhattacharya, A. J. A. W. S. (2017). Drinking water contamination and treatment techniques. *Applied water science*, *7*(3), 1043-1067.
4. Sankhla, M. S., & Kumar, R. (2019). Contaminant of heavy metals in groundwater & its toxic effects on human health & environment. *Available at SSRN 3490718*.
5. Shaji, E., Santosh, M., Sarath, K. V., Prakash, P., Deepchand, V., & Divya, B. V. (2021). Arsenic contamination of groundwater: A global synopsis with focus on the Indian Peninsula. *Geoscience frontiers*, *12*(3), 101079.
6. Sarkar, A., Paul, B., & Darbha, G. K. (2022). The groundwater arsenic contamination in the Bengal Basin-A review in brief. *Chemosphere*, *299*, 134369.
7. Das, T. K. (2019). Arsenic menace in West Bengal (India) and its mitigation through toolbox intervention: an experience to share. *Ground Water Development-Issues and Sustainable Solutions*, 305-314.
8. Singh, A. K. (2006). Chemistry of arsenic in groundwater of Ganges–Brahmaputra river basin. *Current Science*, 599-606.
9. Sen, R., & Sarkar, S. (2019). Arsenic contamination of groundwater in West Bengal: a report. In *Waste Management and Resource Efficiency: Proceedings of 6th IconSWM 2016* (pp. 249-259). Springer Singapore.
10. Mukherjee, A., Fryar, A. E., Eastridge, E. M., Nally, R. S., Chakraborty, M., & Scanlon, B. R. (2018). Controls on high and low groundwater arsenic on the opposite banks of the lower reaches of River Ganges, Bengal basin, India. *Science of the total environment*, *645*, 1371-1387.

11. Guo, X., Qiao, Z., Liu, D., & Zhong, C. (2019). Mixed-matrix membranes for CO 2 separation: Role of the third component. Journal of Materials Chemistry A, 7(43), 24738-24759.
12. Dechnik, J., Gascon, J., Doonan, C. J., Janiak, C., & Sumby, C. J. (2017). Mixed-matrix membranes. Angewandte Chemie International Edition, 56(32), 9292-9310.
13. Bokov, D., Turki Jalil, A., Chupradit, S., Suksatan, W., Javed Ansari, M., Shewael, I. H., ... & Kianfar, E. (2021). Nanomaterial by sol-gel method: synthesis and application. Advances in materials science and engineering, 2021(1), 5102014.
14. Tang, C. Y., & Yang, Z. (2017). Transmission electron microscopy (TEM). In Membrane characterization (pp. 145-159). Elsevier.
15. Halim, J. (2016). An X-ray Photoelectron spectroscopy study of multilayered transition metal carbides (MXenes). Drexel University.
16. Ambroz, F., Macdonald, T. J., Martis, V., & Parkin, I. P. (2018). Evaluation of the BET Theory for the Characterization of Meso and Microporous MOFs. Small methods, 2(11), 1800173.
17. Rouquerol, J., Llewellyn, P., & Rouquerol, F. J. S. S. S. C. (2007). Is the BET equation applicable to microporous adsorbents?. In Studies in surface science and catalysis (Vol. 160, pp. 49-56). Elsevier.
18. Alyamani, A. M. O. L., & Lemine, O. M. (2012). FE-SEM characterization of some nanomaterial. In Scanning electron microscopy. IntechOpen.
19. Kumar, S. P., Balaji, D., & Mandlimath, T. R. (2023). Characterization of flexible ceramics. In Advanced Flexible Ceramics (pp. 25-43). Elsevier.
20. Aremu, J. O., Lay, M., & Glasgow, G. (2019). Kinetic and isotherm studies on adsorption of arsenic using silica based catalytic media. *Journal of Water Process Engineering*, *32*, 100939.
21. Shen, Q., Liu, Z., Hua, Y., Zhao, J., Lv, W., & Mohsan, A. U. H. (2018). Effects of cutting edge microgeometry on residual stress in orthogonal cutting of Inconel 718 by FEM. Materials, 11(6), 1015.
22. Yong, Y., Gu, Y., Ahmad, H. N., Wang, L., Wang, R., & Zhu, J. (2024). Design and characterization of tannic acid/ε-polylysine biocomposite packaging films with excellent

antibacterial and antioxidant properties for beef preservation. Food Chemistry, 439, 138155.

23. Novaes, C. G., Bezerra, M. A., da Silva, E. G. P., dos Santos, A. M. P., da Silva Romao, I. L., & Neto, J. H. S. (2016). A review of multivariate designs applied to the optimization of methods based on inductively coupled plasma optical emission spectrometry (ICP OES). Microchemical journal, 128, 331-346.
24. Gorog, S. (2018). Ultraviolet-visible spectrophotometry in pharmaceutical analysis. CRC press.
25. Yang, X., Zhang, H., Cheng, S., & Zhou, B. (2022). Optimization of the adsorption and removal of Sb (iii) by MIL-53 (Fe)/GO using response surface methodology. *RSC advances*, *12*(7), 4101-4112.
26. Liu, X., Xu, X., Dong, X., & Park, J. (2020). Competitive adsorption of heavy metal ions from aqueous solutions onto activated carbon and agricultural waste materials. Pol. J. Environ. Stud, 29(1), 749-761.
27. Nadig, A. R., Naik, N. S., Padaki, M., Pai, R. K., & Déon, S. (2021). Impact of graphitic carbon nitride nanosheets in mixed-matrix membranes for removal of heavy metals from water. *Journal of Water Process Engineering*, *41*, 102026.
28. Foorginezhad, S., Zerafat, M. M., Mohammadi, Y., & Asadnia, M. (2022). Fabrication of tubular ceramic membranes as low-cost adsorbent using natural clay for heavy metals removal. *Cleaner Engineering and Technology*, *10*, 100550.
29. Adhikary, R., & Mandal, V. (2017). Status of arsenic toxicity in ground water in West Bengal, India: a review. *MOJ Toxicol*, *3*(5), 104-108.
30. Chu, W. B., Yang, J. W., Liu, T. J., Tiu, C., & Guo, J. (2007). The effects of pH, molecular weight and degree of hydrolysis of poly (vinyl alcohol) on slot die coating of PVA suspensions of TiO2 and SiO2. *Colloids and Surfaces A: Physicochemical and Engineering Aspects*, *302*(1-3), 1-10.
31. Li, C., Sun, W., Lu, Z., Ao, X., & Li, S. (2020). Ceramic nanocomposite membranes and membrane fouling: A review. Water Research, 175, 115674.
32. Li, C., Sun, W., Lu, Z., Ao, X., Yang, C., & Li, S. (2019). Systematic evaluation of TiO2-GO-modified ceramic membranes for water treatment: Retention properties and fouling mechanisms. Chemical Engineering Journal, 378, 122138.

33. Zhang, X., Wang, M., Lin, P., Ma, H., Liu, Y., Zhu, Y., & Zhou, Q. (2023). L-Cysteine functionalized halloysite nanotubes/PVDF ultrafiltration membrane for improving anti-fouling performance. *Journal of Environmental Chemical Engineering*, *11*(6), 111400.
34. Banerjee, S., Das, R., & Bhattacharjee, C. (2023). Exceptional arsenic removal using novel mesoporous Mg-Al-Ti ternary composite oxide nanoparticles prepared via self-assembly templating method. *Separation and Purification Technology*, *326*, 124795.
35. Banerjee, S., Das, A., Das, R., & Bhattacharjee, C. (2024). Mesoporous Mg–Al–Ti composite oxide incorporated mixed matrix ultrafiltration membrane with superior multi-heavy metal removal capacity, anti-fouling & anti-microbial property. Journal of Membrane Science, 703, 122836.
36. Mukherjee, R., Bhunia, P., & De, S. (2016). Impact of graphene oxide on removal of heavy metals using mixed matrix membrane. Chemical Engineering Journal, 292, 284-297.
37. He, Y., Ye, H. C., You, T. T., & Xu, F. (2023). Sustainable and multifunctional cellulose-lignin films with excellent antibacterial and UV-shielding for active food packaging. Food Hydrocolloids, 137, 108355.
38. Klein, S. E., Alzagameem, A., Rumpf, J., Korte, I., Kreyenschmidt, J., & Schulze, M. (2019). Antimicrobial activity of lignin-derived polyurethane coatings prepared from unmodified and demethylated lignins. Coatings, 9(8), 494.
39. Antimicrobial susceptibility testing for Helicobacter pylori isolates from Brazilian children and adolescents: comparing agar dilution, E-test, and disk diffusion [J]
40. Li, K., Zhong, W., Li, P., Ren, J., Jiang, K., & Wu, W. (2023). Antibacterial mechanism of lignin and lignin-based antimicrobial materials in different fields. International Journal of Biological Macromolecules, 126281.
41. Prusty, J. S. (2022). Antifungal discovery from plant sources. In Phytoconstituents and Antifungals (pp. 15-33). Academic Press.
42. Haney, E. F., Trimble, M. J., Cheng, J. T., Vallé, Q., & Hancock, R. E. (2018). Critical assessment of methods to quantify biofilm growth and evaluate antibiofilm activity of host defence peptides. Biomolecules, 8(2), 29.
43. Saleh, M., Isik, Z., Belibagli, P., Arslan, H., Gonca, S., Özdemir, S., ... & Dizge, N. (2023). Fabrication of Ag nanoparticles coated leonardite basalt ceramic membrane with

improved antimicrobial properties for DNA cleavage, E. coli removal and antibiofilm effects. Journal of Industrial and Engineering Chemistry, 128, 532-541.

44. Kaur, H., Rosenberg, M., Kook, M., Danilian, D., Kisand, V., & Ivask, A. (2024). Antibacterial activity of solid surfaces is critically dependent on relative humidity, inoculum volume, and organic soiling. FEMS microbes, 5, xtad022.
45. Johari, N. D., Rosli, Z. M., Juoi, J. M., & Yazid, S. A. (2019). Comparison on the TiO2 crystalline phases deposited via dip and spin coating using green sol–gel route. Journal of Materials Research and Technology, 8(2), 2350-2358.
46. Khazaei, A., Nazari, S., Karimi, G., Ghaderi, E., Mansouri Moradian, K., & Bagherpor, Z. (2016). Synthesis and characterization of γ-alumina porous nanoparticles from sodium aluminate liquor with two different surfactants. International Journal of Nanoscience and Nanotechnology, 12(4), 207-214.
47. Khazaei, A., Nazari, S., Karimi, G., Ghaderi, E., Mansouri Moradian, K., & Bagherpor, Z. (2016). Synthesis and characterization of γ-alumina porous nanoparticles from sodium aluminate liquor with two different surfactants. International Journal of Nanoscience and Nanotechnology, 12(4), 207-214.
48. Zavala, M. Á. L., & Bouchez, B. F. (2022). Montmorillonite-perlite-iron ceramic membranes for the adsorption/removal of As (III) and other constituents from surface water. Ceramics International, 48(21), 31695-31704.
49. Evers, S., Yim, T., & Nazar, L. F. (2012). Understanding the nature of absorption/adsorption in nanoporous polysulfide sorbents for the Li–S battery. The Journal of Physical Chemistry C, 116(37), 19653-19658
50. Zhang, X., Fang, X., Li, J., Pan, S., Sun, X., Shen, J., ... & Zhao, S. (2018). Developing new adsorptive membrane by modification of support layer with iron oxide microspheres for arsenic removal. Journal of colloid and interface science, 514, 760-768.
51. Zhang, D., Hu, H., Wei, J. A., Xu, X., Chen, L., Wu, X., ... & Wang, L. (2023). Zr-doped TiO2 ceramic nanofibrous membranes for enhancing photocatalytic organic pollutants degradation and antibacterial activity. Colloids and Surfaces A: Physicochemical and Engineering Aspects, 665, 131231.

52. Yoshida, W., & Cohen, Y. (2003). Ceramic-supported polymer membranes for pervaporation of binary organic/organic mixtures. Journal of membrane science, 213(1-2), 145-157.
53. Shakoor, M. B., Niazi, N. K., Bibi, I., Shahid, M., Saqib, Z. A., Nawaz, M. F., ... & Rinklebe, J. (2019). Exploring the arsenic removal potential of various biosorbents from water. Environment international, 123, 567-579.
54. Mahatmanti, F. W., Jumaeri, J., & Kusumastuti, E. (2023). The adsorption behavior of individual Cu (II), Zn (II), and Cd (II) ions over a CuO-modified ceramic membrane synthesized from fly ash. Journal of King Saud University-Science, 35(8), 102866.
55. Nguyen, C. M., Bang, S., Cho, J., & Kim, K. W. (2009). Performance and mechanism of arsenic removal from water by a nanofiltration membrane. Desalination, 245(1-3), 82-94.
56. Gongping, L. I. U., Wang, W. E. I., Wanqin, J. I. N., & Nanping, X. U. (2012). Polymer/ceramic composite membranes and their application in pervaporation process. Chinese Journal of Chemical Engineering, 20(1), 62-70.
57. Liu, Z., Wang, Z., Zhao, L., Xu, J., Chen, J. P., & Niu, Q. J. (2024). Rod-coated PVA interlayer induced nanofiltration membrane: Method development and application for separation of dye/NaCl with greater performance. Journal of Membrane Science, 694, 122406.
58. Pezeshki, H., Hashemi, M., & Rajabi, S. (2023). Removal of arsenic as a potentially toxic element from drinking water by filtration: a mini review of nanofiltration and reverse osmosis techniques. Heliyon, 9(3).
59. Kim, J., & Van der Bruggen, B. (2010). The use of nanoparticles in polymeric and ceramic membrane structures: review of manufacturing procedures and performance improvement for water treatment. Environmental Pollution, 158(7), 2335-2349.
60. Ashraf, S., Siddiqa, A., Shahida, S., & Qaisar, S. (2019). Titanium-based nanocomposite materials for arsenic removal from water: A review. Heliyon, 5(5).
61. Huang, J., Yuan, F., Zeng, G., Li, X., Gu, Y., Shi, L., ... & Shi, Y. (2017). Influence of pH on heavy metal speciation and removal from wastewater using micellar-enhanced ultrafiltration. Chemosphere, 173, 199-206.

62. Luther, S., Borgfeld, N., Kim, J., & Parsons, J. G. (2012). Removal of arsenic from aqueous solution: A study of the effects of pH and interfering ions using iron oxide nanomaterials. Microchemical Journal, 101, 30-36.
63. Aremu, J. O., Lay, M., & Glasgow, G. (2019). Kinetic and isotherm studies on adsorption of arsenic using silica based catalytic media. Journal of Water Process Engineering, 32, 100939.
64. Liang, D., Huang, J., Zhang, H., Fu, H., Zhang, Y., & Chen, H. (2021). Influencing factors on the performance of tubular ceramic membrane supports prepared by extrusion. Ceramics International, 47(8), 10464-10477.
65. Aremu, J. O., Lay, M., & Glasgow, G. (2019). Kinetic and isotherm studies on adsorption of arsenic using silica based catalytic media. Journal of Water Process Engineering, 32, 100939.
66. Khulbe, K. C., Matsuura, T., Lamarche, G., & Lamarche, A. M. (2000). X-ray diffraction analysis of dense PPO membranes. Journal of Membrane Science, 170(1), 81-89.
67. Shi, M., Li, Z., Yuan, Y., Yue, T., Wang, J., Li, R., & Chen, J. (2015). In situ oxidized magnetite membranes from 316L porous stainless steel via a two-stage sintering process for hexavalent chromium [Cr (VI)] removal from aqueous solutions. Chemical Engineering Journal, 265, 84-92.